

TESTING COLD DARK MATTER MODELS AT MODERATE TO HIGH REDSHIFT

RENYUE CEN¹

Draft version August 17, 2018

ABSTRACT

The COBE microwave background temperature fluctuations and the abundance of local rich clusters of galaxies provide the two most powerful constraints on cosmological models. When all variants of the standard cold dark matter (CDM) model are subject to the combined constraint, the power spectrum of any model is fixed to $\sim 10\%$ accuracy in both the shape and overall amplitude. These constrained models are not expected to differ dramatically in their local large-scale structure properties. However, their evolutionary histories differ, resulting in dramatic differences towards high redshift. In particular, it should be true that any statistical measure that probes a rapidly diminishing tail of some distribution should provide a sensitive test at some sufficiently high redshift, when the objects in question are rare and hence in the tail.

We examine in detail six standardized, COBE and cluster normalized CDM models with respect to a large set of independent observations. The observations include correlation function of rich clusters of galaxies, galaxy power spectrum, evolution of rich cluster abundance, gravitational lensing by moderate-to-high redshift clusters, Ly α forest, damped Ly α systems, high redshift galaxies, reionization of the universe and future CMB experiments. It seems that each of the independent observations examined is or potentially is capable of distinguishing between at least some of the models. The combined power of several or all of these observations is tremendous. Thus, we appear to be on the verge of being able to make dramatic tests of all models in the near future using a rapidly growing set of observations, mostly at moderate to high redshift. Consistency or inconsistency between different observed phenomena on different scales and/or at different epochs with respect to the models will have profound implications for theory of growth of cosmic structure.

Subject headings: Cosmology: large-scale structure of Universe – cosmology: theory – galaxies: clustering – galaxies: formation – numerical method

1. INTRODUCTION

On one hand, the success of the COsmic microwave Background Explorer (COBE; Smoot et al. 1992) can hardly be overstated; it revolutionized our way of quantifying cosmology. On the other hand, it did little justice to enthusiastic cosmologists: rather than helping us nail down to an ultimate model, it prodded us to introduce more models (or variants) to meet with the new observational constraint. Post-COBE era is filled with new ideas about models at the expense of introducing more parameters to the simple, non-flavored, standard cold dark matter model (Peebles 1982; Blumenthal et al. 1984), which has been remarkably successful in matching a large set of local observations for the past decade (e.g., Davis et al. 1985; White et al. 1986; Frenk et al. 1988; Park 1990; Cen & Ostriker 1992a and references therein), although some evidence of its lack of large-scale power began to emerge (e.g., Maddox et al. 1990) in the early nineties (see Ostriker 1993 for an excellent review). The flourish of new models is largely thanks to the general consensual requirement that any cosmological model match both the COBE observation on large scales at an early epoch and local observations, primarily of distributions of galaxies.

The newly introduced models that are deemed to be interesting are mostly based on the general success of the standard cold dark matter model. The variants arise by introducing one or two more parameters to the standard critical density CDM model with Zel'dovich primordial

spectrum: the shape of the power spectrum (characterized by the primordial power index on the large scales, n) and/or the composition of the universal matter including vacuum energy density (cosmological constant). It should be noted that variations of the latter also change the overall shape of the power spectrum, quite separate from the primordial spectrum. The consequence of allowing such added freedom is the current state of a degenerate set of “viable” COBE and cluster-normalized CDM models typified by the tilted cold dark matter model (Cen et al. 1992, Liddle, Lyth, & Sutherland 1992; Lidsey & Coles 1992; Adams et al. 1993; Lucchin, Matarrese, & Mollerach 1992), the mixed cold dark matter model (Davis, Summers & Schlegel 1992; Taylor & Rowan-Robinson 1992; Klypin et al. 1993; Cen & Ostriker 1994a; Ma & Bertschinger 1994), the cold dark matter model with a non-zero cosmological constant (Peebles 1984; Efstathiou, Bond, & White 1992; Kofman et al. 1993; Cen, Gnedin, & Ostriker 1993; Ostriker & Steinhardt 1995) and the open cold dark matter model (Gott 1982; Bucher, Goldhaber, & Turok 1995). Although noticeably being paid significantly less attention to, the primeval baryon isocurvature model (PBI, Peebles 1987a,b; Cen, Ostriker, & Peebles 1993) still appears contentious, especially with its virtue of early structure formation.

After a general world model is chosen (i.e., Ω_0 , Λ_0 , H_0 and dark matter and baryonic compositions are chosen), the shape and the overall amplitude of its power spectrum

¹Princeton University Observatory, Princeton University, Princeton, NJ 08544; cen@astro.princeton.edu

are yet to be fixed before the model becomes completely deterministic. COBE provides one fixing point at large scales ($\lambda \sim 1000h^{-1}\text{Mpc}$). The abundance of local rich clusters of galaxies provides another fixing point at intermediate scales ($\lambda \sim 10h^{-1}\text{Mpc}$). Both points are currently determined to an accuracy of $\sim 10\%$. Once the power spectrum is also fixed, the entire history of a model universe can, in principle, be computed. Sufficiently accurate numerical techniques with sufficiently realistic physical modeling have become more available due to parallel advances in both computer hardware and software capabilities to allow for accurate predictions for at least some aspects or phenomena of the cosmic structure formation to be made, which can be compared to observations on various scales and at various epochs. Examples are Ly α clouds (Cen et al. 1994; Zhang et al. 1995; Hernquist et al. 1996; MCOR), X-ray clusters (Kang et al. 1994; Bryan et al. 1994; Cen & Ostriker 1994a; Frenk et al. 1998) and gravitational lensing by clusters of galaxies and large-scale structure (Cen et al. 1994; Wambsganss et al. 1995).

Parallel in time, rapid advances in observational capabilities in recent years, thanks in large part to the ground-based 10-meter class Keck telescopes as well as the Hubble Space Telescope (HST), make possible explore regimes which were previously inaccessible. For example, HST opens a brand new window to studying the formation and evolution of galaxies to a much higher redshift than before (e.g., Lowenthal et al. 1997) and quasar absorption systems at some entirely new wavelength bands (e.g., Bahcall et al. 1996). Observations by Keck telescopes have made possible routinely record high quality quasar absorption spectra (e.g., Hu et al. 1995), providing new opportunities to conduct detailed studies of Lyman alpha forest lines and related metal line systems (e.g., Lu et al. 1997). Observations of Lyman break galaxies using Keck telescopes have opened yet another new window to the universe at high redshift (Steidel et al. 1998, S98 henceforth). Deeper and larger surveys of X-ray clusters of galaxies as well as optically identified clusters of galaxies are pushing the redshift of observed rich, luminous and hot clusters to beyond unity (e.g., Rosati et al. 1998). More excitingly, more and rapid observational advances are expected to take place in the near future in anticipation of many large projects and next generation telescopes covering a variety of wavelengths from meterwave to γ -ray.

This paper attempts to interface between these two developments. To set a standard for comparing different models and for comparing results between different workers in the field, we adopt the set of six CDM models presented in Cen (1998; C98 henceforth) for detailed analyses. All the models are normalized to both COBE on large scales and the observed abundance of local rich clusters of galaxies, thus titled “viable”. The goal of this paper is to address the opportunities that new observations are and will soon be providing us with new ways to test these remaining, “viable” models. It is hoped that some theoretical insight may be extracted to help highlight some potentially promising observations for (at least) the purpose of testing cosmological models. It is exciting that each of the independent observations examined here, mostly at moderate-to-high redshift, seems to be or potentially be capable of distinguishing between at least some of the models. The combined power of several of these obser-

vations is tremendous, enabling the possibility of nailing down the ultimate cosmological model with high precision. It is perhaps more important that different observations at completely different scales and/or epochs should provide an overall consistency check of the general gravitational instability picture and/or Gaussianity of the primordial density fluctuations.

The main results of the paper are organized as follows. The parameters of a suite of six CDM models that are normalized to COBE and local cluster abundance are discussed in §2. §3 presents tests on the models with nine independent observations in order of ascending redshift in the subsections: the cluster correlation function (§3.1), the galaxy power spectrum from the Sloan Digital Sky Survey (SDSS) (§3.2), the evolution of rich cluster abundance (§3.3), the gravitational lensing by moderate-to-high redshift clusters of galaxies (§3.4), the Ly α forest (§3.5), the damped Ly α systems (§3.6), the high redshift galaxies (§3.7), the reionization of the universe (§3.8) and the future CMB experiments (§3.9). Discussion of the constraining/differentiating power and observational requirement of each of the suite of observations is presented in §4. Conclusions are given in §5.

2. SIX COBE AND CLUSTER NORMALIZED CDM MODELS

The models are taken from C98 (Table 4 of that paper) and listed in Table 1. When normalized to both COBE on very large scales and the abundance of local rich clusters of galaxies, both the shape (n) and amplitude of the power spectrum (σ_8) of any model are fixed to about 10% accuracy (C98). These six models are determined to this accuracy. The Λ CDM model has $\Omega_0 = 1$ but with a tilt on the primordial power spectrum. The HCDM model has $\Omega_0 = 1$ with 20% mass in massive neutrinos. Two neutrino species of equal mass are assumed. OCDM25 and OCDM40 are two open models and Λ CDM25 and Λ CDM40 are two low density but flat models with a cosmological constant. Except the open models, a tensor component is added when normalizing each model to COBE with tensor to scalar ratio $T/S = 7(1 - n)$ (Liddle & Lyth 1992; Davis et al. 1992; Crittenden et al. 1993; Stewart & Lyth 1993). Note that some tilt is present in all models listed, required to match both COBE and local cluster abundance. This set of six CDM models likely brackets all potentially interesting models.

The baryon densities for OCDM25 and Λ CDM25 are computed using $\Omega_b h^2 = 0.0125$ (Walker et al. 1991), and for the remaining four models using $\Omega_b h^2 = 0.0193$ (Burles & Tytler 1997). These choices of Ω_b for the models are made to maximize the viability of each model with respect to the observed gas fraction in X-ray clusters of galaxies (White et al. 1993b; Lubin et al. 1996; Danos & Pen 1998, $\rho_{gas}/\rho_{tot} = (0.053 \pm 0.004)h^{-3/2}$). The power spectrum transfer functions for all the models are computed using CMBFAST code developed by Seljak and Zaldarriaga. The choice of the Hubble constant is made for each model such that each model is consistent with current measurements of the Hubble constant. It appears that $H_0(obs) = 65 \pm 10 \text{ km/s/Mpc}$ can account for the distribution of the current data from various measurements (see, e.g., Trimble 1997), except for those from Sunyaev-Zel’dovich observations (for a discussion of a reconcilia-

TABLE 1
SIX COBE AND CLUSTER-NORMALIZED CDM MODELS

Model	H_0	n	Ω_c	Ω_b	Λ_0	Ω_b	σ_8
tCDM	55	0.77	0.936	0.00	0.0	0.064	0.55
HCDM	55	0.88	0.736	0.20	0.0	0.064	0.52
OCDM25	65	1.47	0.220	0.00	0.0	0.030	1.00
OCDM40	60	1.15	0.346	0.00	0.0	0.054	0.80
Λ CDM25	65	1.10	0.220	0.00	0.75	0.030	0.95
Λ CDM40	60	0.96	0.346	0.00	0.60	0.054	0.80

Figure 1

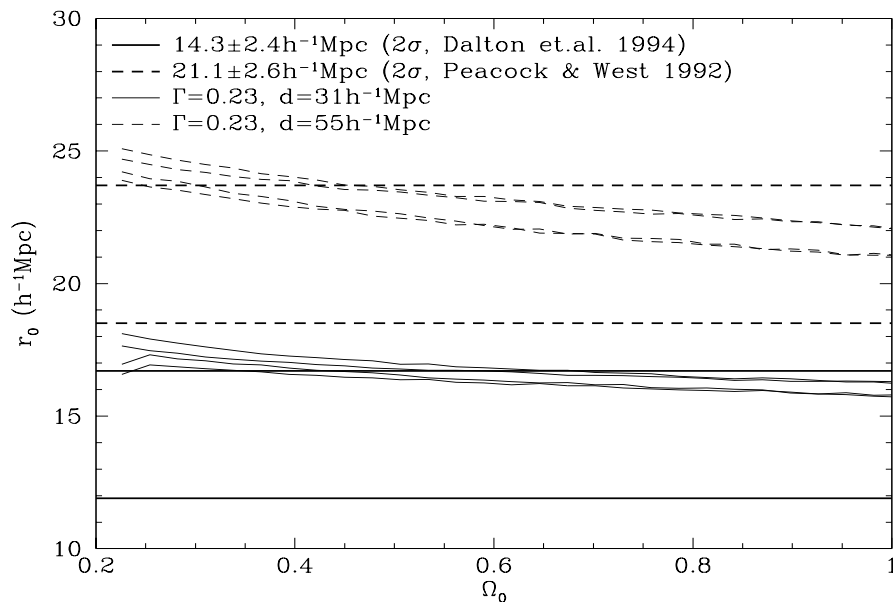


FIG. 1.— Cluster-cluster two-point correlation length computed using GPM as a function of Ω_0 for clusters with mean separation of $55h^{-1}\text{Mpc}$ (light dashed curves) and $31h^{-1}\text{Mpc}$ (light solid curves), respectively. For all models we use the CDM transfer function from BBKS with $\Gamma \equiv \Omega_0 h = 0.23$ and $n = 1.0$. All models are normalized to clusters using equation 36 of C98. Each set of four curves consists of two upper curves using 2σ upper limit of σ_8 by equation 36 of C98 with $\Lambda_0 = 0$ and with $\Omega_0 + \Lambda_0 = 1$, and two lower curves using 2σ upper limit of σ_8 with $\Lambda_0 = 0$ and with $\Omega_0 + \Lambda_0 = 1$. Also shown as two heavy dashed horizontal line indicate the 2σ upper and lower bounds from observations by Peacock & West (1992) of the correlation length of clusters of mean separation of $55h^{-1}\text{Mpc}$. The two heavy solid horizontal lines are the 2σ upper and lower bounds from observations by Dalton et al. (1994) of the correlation length of clusters of mean separation of $31h^{-1}\text{Mpc}$.

tion of this difference, see C98). Another consideration is that the age constraint from latest globular cluster observations/interpretations (c.f., Salaris, Degl'Innocenti, & Weiss 1997) is not violated.

3. TESTING CDM MODELS AT MODERATE TO HIGH REDSHIFT

While COBE and local cluster abundance combine to provide an unprecedented accuracy of fixing models in terms of limiting the parameter space, some degeneracy remains. It is therefore essential to examine other, independent observations to help further tighten the parameter space. We will examine various observations in this section using the six models listed in Table 1 as a testbed. We consider nine independent observations in order of ascending redshift: the cluster correlation function at low redshift (§3.1), the galaxy power spectrum from SDSS (§3.2), and evolution of rich cluster abundance (§3.3), the gravitational lensing by moderate-to-high redshift clusters of galaxies (§3.4), the Ly α forest (§3.5), the damped Ly α systems (§3.6), the high redshift galaxies (§3.7), the reionization of the universe (§3.8) and the future CMB experiments (§3.9).

3.1. Constraints by the Cluster Correlation Function at $z = 0$

Before examining the correlation functions of the six models, it is worthwhile to understand factors that determine the cluster correlation function. Figure 1 shows the cluster-cluster two-point correlation length (i.e., the scale at which the correlation function is unity), computed using the Gaussian Peak Method (GPM, C98), as a function of Ω_0 for clusters with mean separation of $55h^{-1}\text{Mpc}$ (light dashed curves) and $31h^{-1}\text{Mpc}$ (light solid curves), respectively. For all models shown here, we use $\Gamma = 0.23$ with the CDM transfer function from BBKS and normalize to the local cluster abundance (equation 36 of C98) but not necessarily to COBE. From Figure 1 it immediately becomes clear that the cluster correlation function almost does not depend on Λ_0 at all, only weakly depends on Ω_0 and somewhat moderately depends on σ_8 : $dr_0/d\Lambda_0 \approx 0$, $dr_0/d\Omega_0 \approx 2 - 4$, and $dr_0/d\sigma_8 \approx 6 - 10$. Therefore, given the uncertainties in fixing σ_8 of a model, uncertainties in the shape of the power spectrum and uncertainties in the observed correlation length of clusters, it is not possible to constrain Ω_0 using correlation functions of clusters of galaxies, *unless models with different Ω_0 also substantially differ in P_k on the relevant large scales ($30 - 300h^{-1}\text{Mpc}$).*

Fortunately, the power spectra of various models with different Ω_0/Λ_0 are indeed quite different (Table 1), as required to fit both COBE and local rich cluster abundance. Figure 2 shows the power spectra (in real space) for the six models in Table 1. It is seen that normalizing to both COBE and clusters results in a wide disparity in shape and amplitude of the power spectra of the models in a wide range of scales. The correlation length of clusters of galaxies in the six models are then shown in Figure 3 in a somewhat different manner, where the correlation length in each model is plotted against the mean separation of the clusters in question. Note that the mean separation of a set of clusters is the mean separation of a set of the richest (most massive) clusters in a model; clusters are rank-ordered in mass and selected in descending

order in mass. We see that there exists significant differences between different models shown here. Since we have explicitly shown earlier that the dependence of the correlation length on Ω_0 and Λ_0 is rather weak, the differences in the correlation lengths between the models shown here chiefly attribute to the differences in the power on large scales between the models. The trend is clear and physically understandable: the more power a model has on large scales $\lambda \geq 100h^{-1}\text{Mpc}$, the stronger dependence of the correlation length on the richness of the clusters (see Figure 2 to compare the power spectra of the models) is displayed, consistent with previous findings (Bahcall & Cen 1992; Croft & Efstathiou 1994).

It is evident that the correlation length of clusters of galaxies sets a useful constraint on models. If the measurement accuracy can reach $\leq 1h^{-1}\text{Mpc}$, one can potentially strongly differentiate between models. It is also clear that it will be more useful to reduce the observational errorbars of the correlation length of very rich clusters (e.g., $d \geq 90h^{-1}\text{Mpc}$) for the purpose of testing models, since the models differ most there. Stated somewhat more quantitatively in a hypothetical sense, were the 2σ errorbar of the solid dot in Figure 3 smaller than $5h^{-1}\text{Mpc}$, all the models considered here are ruled out at a very high confidence level ($\sim 4\sigma$).

Consistent with other observations (e.g., Maddox et al. 1990) and previous results of clustering analyses of galaxy clusters (e.g., Bahcall & Cen 1992; Croft & Efstathiou 1994), the standard $\Omega_0 = 1$ CDM model even with a significant tilt of the power spectrum ($n = 0.77$, tCDM) is in disaccord with currently available observations due to the lack of large-scale power. HCDM model and all other, low density models are consistent with available observations of cluster correlations.

3.2. Galaxy Power Spectrum

The Sloan Digital Sky Survey now underway (Knapp, Lupton, & Strauss 1996) will provide a tremendously large database for a variety of objects. Realizing its full value will perhaps require the work by generations of astronomers. One obviously valuable piece of information that can be extracted immediately upon the availability of the distribution of galaxies from SDSS, up to very large scales previously unreachable in full three dimension. Figure 4 shows the power spectra of galaxies for the six models (Table 1) *in redshift space* at $z = 0$. The shown galaxy power spectrum in redshift space for each model is related to the linear matter power spectrum in real space by the following relation:

$$P_{gal,red}(k) = \left(1 + \frac{2}{3}\Omega_0^{0.6} + \frac{1}{5}\Omega_0^{1.2}\right)\sigma_8^{-2}P_{mass,real}(k). \quad (1)$$

In the above relation the first term on the right hand side is due to linear peculiar velocity distortion (Kaiser 1987) and the second term on the right hand side reflects the (linear) bias of galaxies over mass in order for each model to be consistent with the observed galaxy density fluctuations at $z=0$. For tCDM, we also show the errorbars (2σ) that SDSS can achieve, adopted from Goldberg & Strauss (1998). Errorbars for other models are the same but not shown for readability of the figure. It is clear that the SDSS galaxy power spectrum in a large range

Figure 2

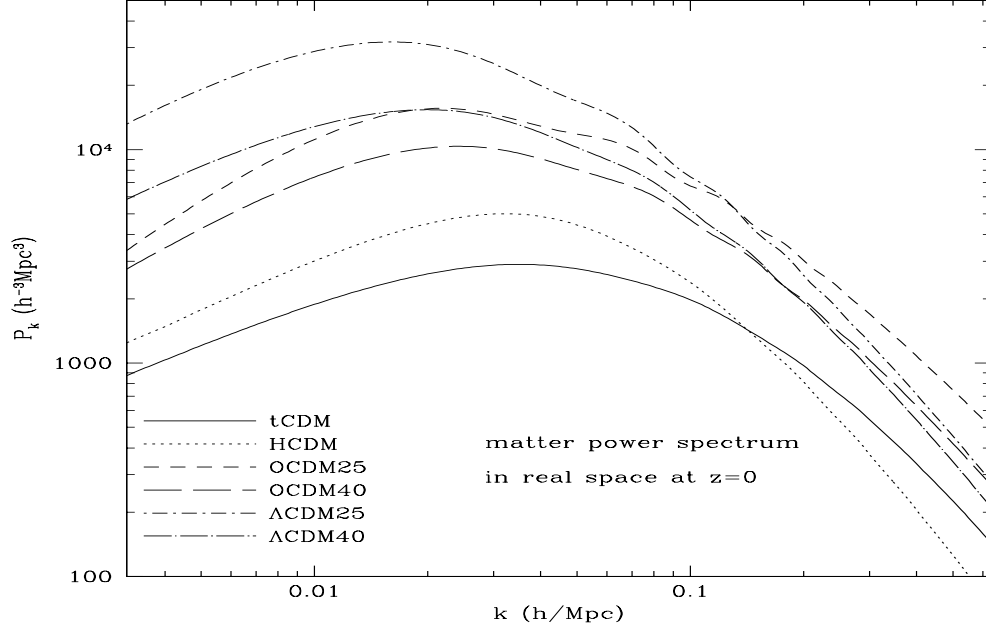


FIG. 2.— shows the power spectra (in real space) for the six models in Table 1.

Figure 3

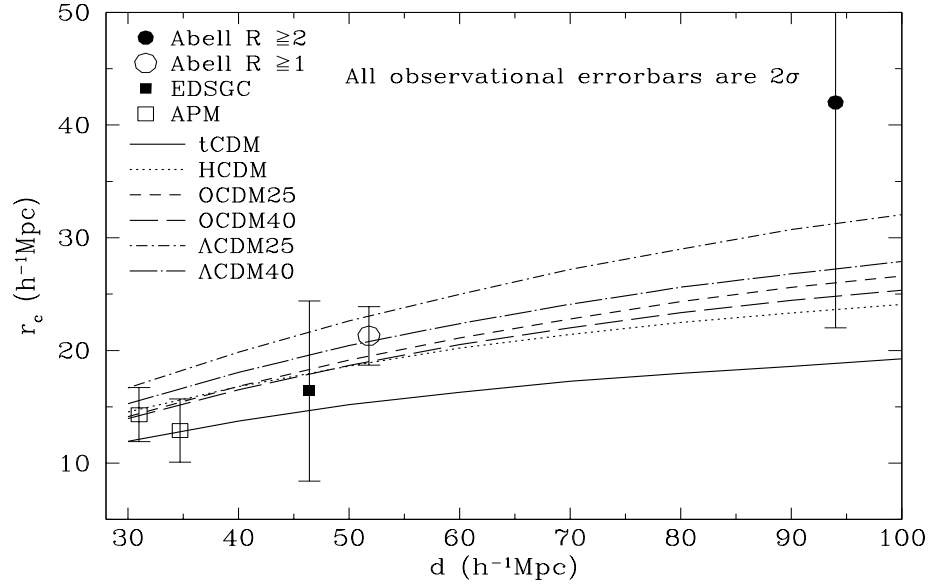


FIG. 3.— shows the correlation length against the mean separation of the clusters in the six models (Table 1). Shown as symbols are observations from various sources, where the filled dot is for $R \geq 2$ Abell clusters from Bahcall & Soneira (1983) with separation $d = 94h^{-1}\text{Mpc}$ and correlation length $r_0 = 42 \pm 20h^{-1}\text{Mpc}$, the open circle is for $R \geq 1$ Abell clusters from Peacock & West (1992) with separation $d = 51.8h^{-1}\text{Mpc}$ and correlation length $r_0 = 21.3 \pm 2.6h^{-1}\text{Mpc}$, the solid square is for Edinburgh-Durham Southern Galaxy Catalogue (EDSGC) from Nichol et al. (1992) with separation $d = 46.4h^{-1}\text{Mpc}$ and correlation length $r_0 = 16.4 \pm 8.0h^{-1}\text{Mpc}$, and the two open squares are for APM Galaxy survey from Dalton et al. (1992) with separation $d = 34.7h^{-1}\text{Mpc}$ and correlation length $r_0 = 12.9 \pm 2.8h^{-1}\text{Mpc}$ and from Dalton et al. (1994) with separation $d = 31.0h^{-1}\text{Mpc}$ and correlation length $r_0 = 14.3 \pm 2.4h^{-1}\text{Mpc}$. All the observational error bars are 2σ .

Figure 4

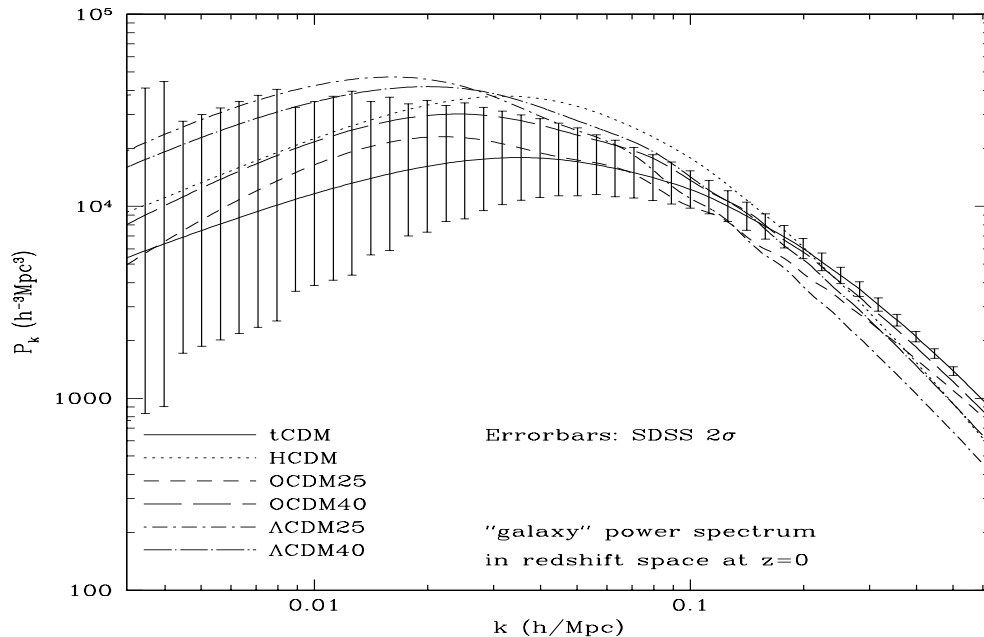


FIG. 4.— The power spectra of galaxies *in redshift space* for the six models (Table 1) at $z = 0$. See text for how they are obtained. For tCDM, we also show the errorbars (2σ) that SDSS are thought to achieve, adapted from Goldberg & Strauss (1998).

in k from $0.01 h/\text{Mpc}$ to $0.5 h/\text{Mpc}$ will provide some discriminatory tests of the models. Taken at face value, it seems that the errorbars are smallest at the highest k , where the data points may provide the most discriminating test of the models. But we caution that nonlinear effects may wash out some of the differences between the models at the high k end (e.g., Gramann, Cen & Bahcall 1993). We should only conservatively estimate the discriminating power of the galaxy power spectrum from SDSS at $k < 0.2 h/\text{Mpc}$, where the nonlinear effects are relatively mild. A close examination of Figure 4 reveals that there is not a pair of models that have the same power at $k < 0.2 h/\text{Mpc}$ within the 2σ errorbars provided by SDSS. Therefore, SDSS should be able to test all these models at a confidence level $> 2\sigma$. The purpose of this investigation is to illustrate the potential of SDSS galaxy power spectrum in placing strong constraints on models. Quantitative comparisons will have to be made between large-scale, fully nonlinear cosmological galaxy formation simulations (Cen & Ostriker 1992b, 1993b, 1998) and observations.

3.3. Evolution of Cluster Mass Function

Let us now study the evolution of the cluster mass functions in the six models (Table 1), computed using GPM (C98). Figure 5 displays the mass functions for the models at four redshifts, $z = 0.0, 0.3, 0.5, 1.0$. The cluster mass is defined as the mass in a sphere of *comoving* Abell radius ($r_A = 1.5 h^{-1} \text{Mpc}$) at all redshifts. Again, *all models are normalized to the observed mass function at redshift zero as well as COBE*. As one would have naively expected, the evolution is strongest in the $\Omega_0 = 1$ models (5a,b) and

weakest in the open, lowest density model (5c). It must be stressed, however, as we will show shortly, that the physical reason for this trend may come as a surprise. *The underlying cause is σ_8 , not Ω_0* . The HCDM (5b) shows a comparable rate of evolution to tCDM (5a) because the reduction of power on smaller scales $k > 0.12 h/\text{Mpc}$ is roughly compensated by a comparable increase of power on larger scales $k < 0.12 h/\text{Mpc}$ in HCDM compared to tCDM. Other models show intermediate rates of evolution, in a comprehensible order. Figure 6 is similar to Figure 5 with the only difference being that the cluster mass is now defined as the mass in a sphere of *proper* Abell radius ($r_A = 1.5 h^{-1} \text{Mpc}$) at all redshifts. The trend between models is similar in Figure 6 to that in Figure 5. But the evolutionary rates in all models are dramatically smaller in Figure 6 than in Figure 5. This says that the mass of clusters within a physical radius evolves much more slowly than the mass of clusters within a comoving radius. This is trivial, since a fixed physical radius corresponds to a larger comoving radius at a higher redshift thus its sphere contains more mass than its counterpart with the comoving radius. A more subtle difference between the models is that the evolution of the mass function for the low density open model (OCDM25) to redshift unity (the bottom curve in Figure 6c) is much smaller than that of any other model. In other words, the mass of clusters within a physical radius in OCDM25 evolves only very slowly. An equivalent, conventional but perhaps conceptually simpler way to put this is that the clusters in OCDM25 virialize early at $z \sim 1$ and later mass accretion onto the formed clusters through the surface of the indicated radius is modest.

We would summarize the trends for clarity. *Clus-*

Figure 5

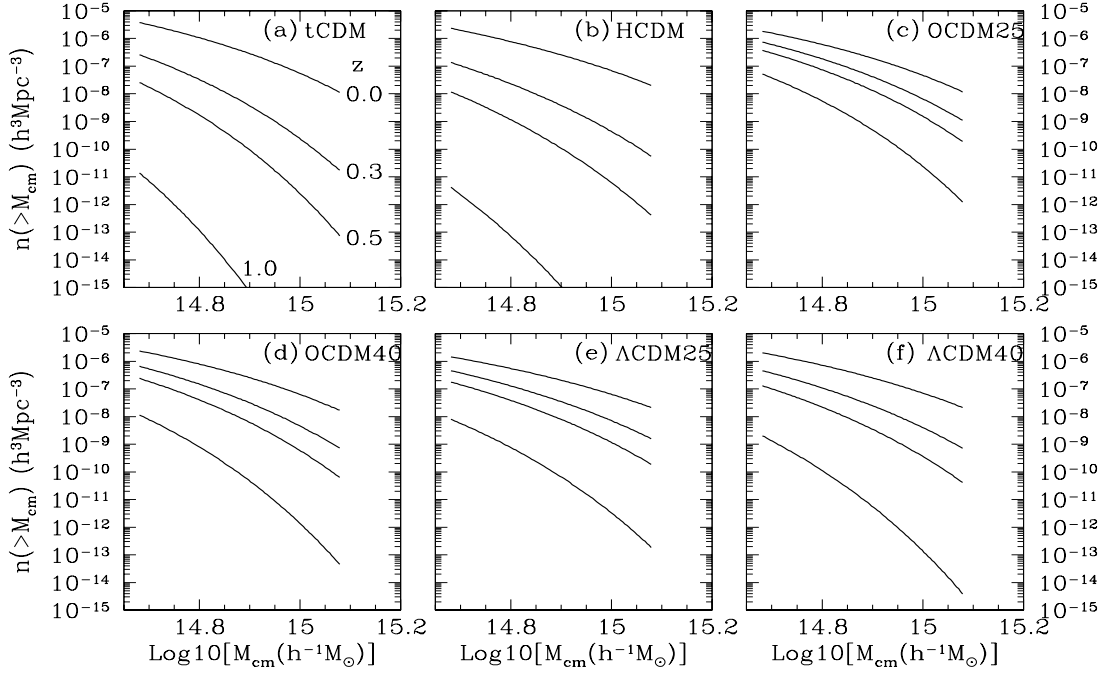


FIG. 5.— It displays the mass functions for the models at four redshifts, $z = 0.0, 0.3, 0.5, 1.0$. The cluster mass is defined as the mass in a sphere of *comoving* Abell radius ($r_A = 1.5 h^{-1} \text{Mpc}$) at all redshifts. All models are normalized to the observed mass function at redshift zero.

Figure 6

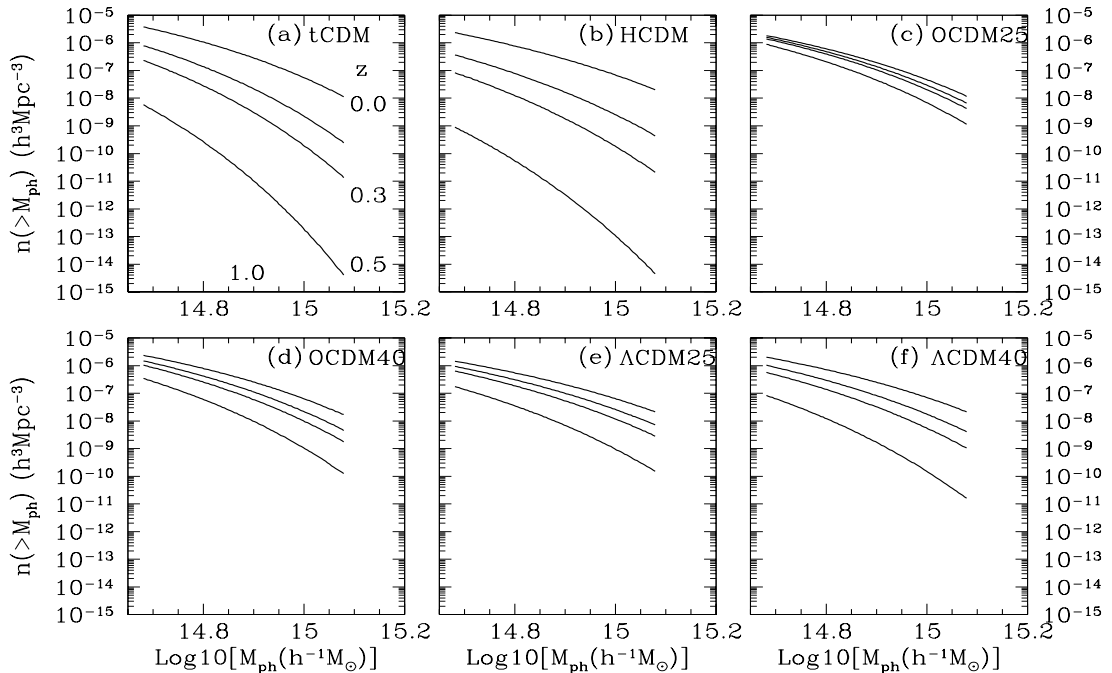


FIG. 6.— is similar to Figure 5 with the only difference being that the cluster mass is defined as the mass in a sphere of *proper* Abell radius ($r_A = 1.5 h^{-1} \text{Mpc}$) at all redshifts.

ter mass function is a monotonic function in time: the abundance of clusters at a fixed mass (at least in the range of mass considered here from $4.8 \times 10^{14} h^{-1} M_{\odot}$ to $1.2 \times 10^{15} h^{-1} M_{\odot}$) decreases with increasing redshift. For all COBE and cluster (at $z = 0$) normalized models, the lower is Ω_0 , the weaker is the evolution; for two models with a same Ω_0 , an addition of a cosmological constant enhances the evolution, especially beyond a certain high redshift when the values of Ω_z in the two models (with and without a cosmological constant) start to deviate significantly from one another. However, it is worth noting that the faster evolution in the low density models than in the high density models is somewhat coincidental (due to $\sigma_8 - \Omega_0$ relation required to fit local rich cluster abundance, equation 36 of C98) and entirely due to the normalization on σ_8 , not due to Ω_0 , as will be shown below.

Presenting the above results shown in Figures (5,6) in a slightly different form, panel (a) of Figure 7 shows the evolution of the number of clusters with mass of $\geq 5.6 \times 10^{14} h^{-1} M_{\odot}$ within a fixed proper radius of $1.5 h^{-1} \text{Mpc}$, and panel (b) of clusters with mass of $\geq 7.9 \times 10^{14} h^{-1} M_{\odot}$. The quantity in the ordinate is the number of clusters per unit redshift per unit steradian. Since the number of clusters per unit redshift *per unit solid angle* is plotted, one has to take account the different geometries in different model universes (the comoving volume element per steradian per unit redshift about z is $D_A(z)^2 dr_{cm}(z)/dz$, where D_A is the comoving angular diameter distance to redshift z and $r_{cm}(z)$ is the comoving distance to redshift z ; see equations 6, 8 below for definitions of D_A and r_{cm}). It is seen that the less massive, low redshift clusters shown in panel (a) has much less discriminating power than the more massive, higher redshift clusters shown in panel (b). While the observed clusters at $z = 0.18 - 0.35$ (panel a) are not able to differentiate between any models at a significant confidence level, the observed clusters at $z = 0.35 - 0.55$ and $z = 0.55 - 0.85$ (panel b) offer a clean way to separate the $\Omega_0 = 1$ models from the rest. It seems quite secure to conclude that both $\Omega_0 = 1$ tCDM and HCDM models are ruled out at a high confidence level ($> 3\sigma$), whereas the current observations are not able to differentiate between the four low density models. This conclusion is in broad agreement with the conclusions drawn by Henry & Arnaud (1991), Bahcall, Fan & Cen (1997) and Carlberg et al. (1997). Reichart et al. (1998) claim that the X-ray cluster luminosity function from Einstein Medium Sensitivity Survey are consistent with $\Omega_0 = 1$. It is unclear at this time what causes the difference. However, Reichart et al. (1998) claim that their conclusion is independent of σ_8 (i.e., the amplitude of the power spectrum), which is in direct conflict with the demonstration that σ_8 is the primary factor that determines the redshift evolution of massive clusters, as shown below.

To quantify the power of high redshift X-ray clusters for differentiating between models, we tabulate in Table 2 the expected number of clusters in each of the six models at redshifts greater than 0.5, 1.0 and 2.0, respectively, for clusters with temperatures greater than 0.5keV and 7.0keV, respectively. The numbers are obtained assuming that a survey covering π steradian (i.e., one quarter of the sky) is available. Next generation X-ray telescopes should be able to detect 7keV clusters at $z = 1$ without much difficulty, if clusters at high redshift are *not significantly*

less luminous than their local counterparts at a fixed temperature (e.g., Henry 1997). It is clear from Table 2 that $\Omega_0 = 1$ models are easily differentiated from other models. The subtlety lies in low density models and some degeneracy exists between open models and flat models with cosmological constants. For example, OCDM40 ($\Omega_0 = 4.0$, $\Lambda_0 = 0.0$) and Λ CDM25 ($\Omega_0 = 0.25$, $\Lambda_0 = 0.75$) give comparable number of bright X-ray clusters at $z < 1.0$; but the difference is gradually larger at higher redshift (a factor about four at $z = 2$). Aside from this degeneracy, the database from a survey of the indicated sky coverage should be able to determine Ω_0 with an uncertainty of $\Delta\Omega_0 = 0.02$ (1σ), if $\Omega_0 + \Lambda_0 = 1$ [obtained by assuming statistical (Poisson) errors for the clusters with $kT = 7\text{keV}$ at $z > 1$ of the last two models in Table 2, which exhibit the smallest difference and thus are most demanding]. If the universe is open, one will be able to determine Ω_0 with an accuracy of $\Delta\Omega_0 = 0.008$ (by interpolating between OCDM25 and OCDM40). These accuracies are comparable to those which will be determined from the next generation microwave background fluctuation experiments (e.g., Zaldarriaga, Spergel, & Seljak 1997), thus provide a very powerful test and also a very important consistency cross-check.

So far we have shown that there are dramatic differences in the number density of massive clusters at high redshift between the considered models, when all are normalized to give the same cluster density at $z = 0$. In other words, the rate of evolution for cluster abundance is strongly model-dependent. It is useful to understand what cause such dramatic differences in the evolution rates between the different models. For this let us first define an evolution rate of cluster (with mass $> M$) number density as a function of σ_8 as

$$\mathcal{E}(\sigma_8, > M) \equiv -\frac{d \log_{10} n(\sigma_8, > M)}{dz}. \quad (2)$$

This is the change of cluster abundance in logarithmic scale per unit redshift. This definition is similar to that defined in Fan, Bahcall, & Cen (1998; equation 8) but with the difference that the current \mathcal{E} is a function of σ_8 and M , not a function of z and M . In this sense the current definition of rate of evolution is local in time; redshift z in equation 2 serves as a ruler or a unit. Figure 8a shows the evolution rate of the number density of clusters with mass $> 5.6 \times 10^{14} h^{-1} M_{\odot}$, defined within a comoving Abell radius (panel a) and within a physical Abell radius (panel b), respectively. The first thing to notice is that, not surprisingly, the evolution rate is lower for clusters defined within a physical Abell radius than within a comoving Abell radius. Secondly, *the differences between models at a fixed σ_8 are smaller than the differences of any single model at different σ_8 's*. For example, for OCDM25 \mathcal{E} changes from 1.4 to 6.8 for σ_8 from 1.0 to 0.5, while the differences in \mathcal{E} between tCDM and OCDM25 is 0.6 at $\sigma_8 = 1.0$ and 2.0 at $\sigma_8 = 0.5$. However, it is interesting to note that, *at a fixed σ_8 , the evolution rates in the low Ω_0 models are higher, not lower, than the rates in the $\Omega_0 = 1$ models for clusters defined within the comoving Abell radius (panels a)*. The situation is altered for clusters defined within the physical Abell radius: *at a fixed σ_8 , the evolution rate is lowest in OCDM25*. In any case these differences are secondary compared to the difference of \mathcal{E} between differ-

Figure 7

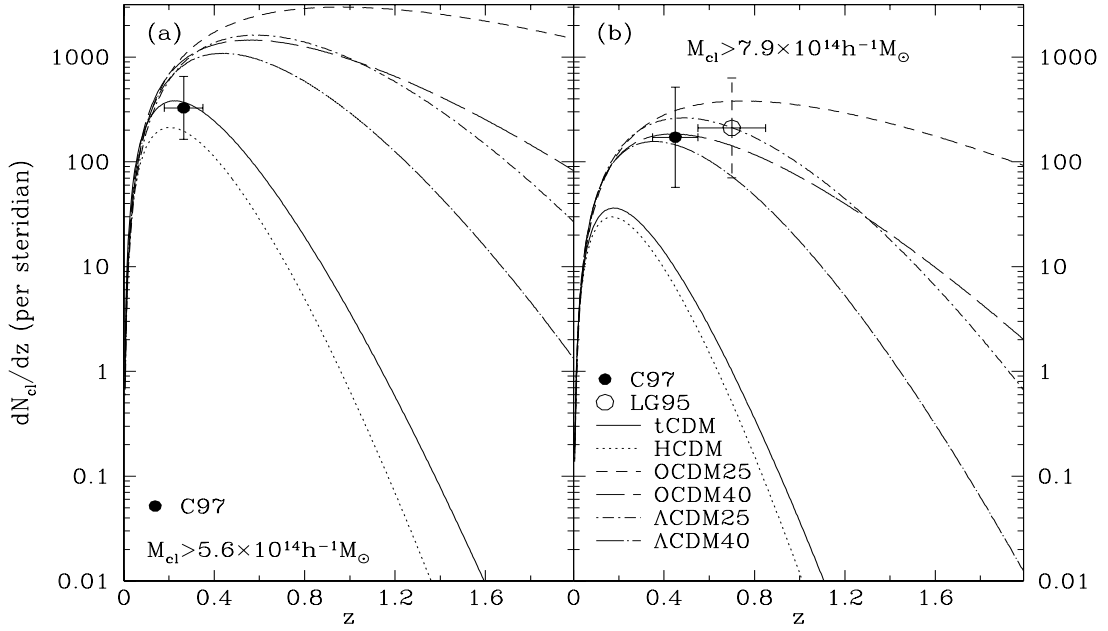


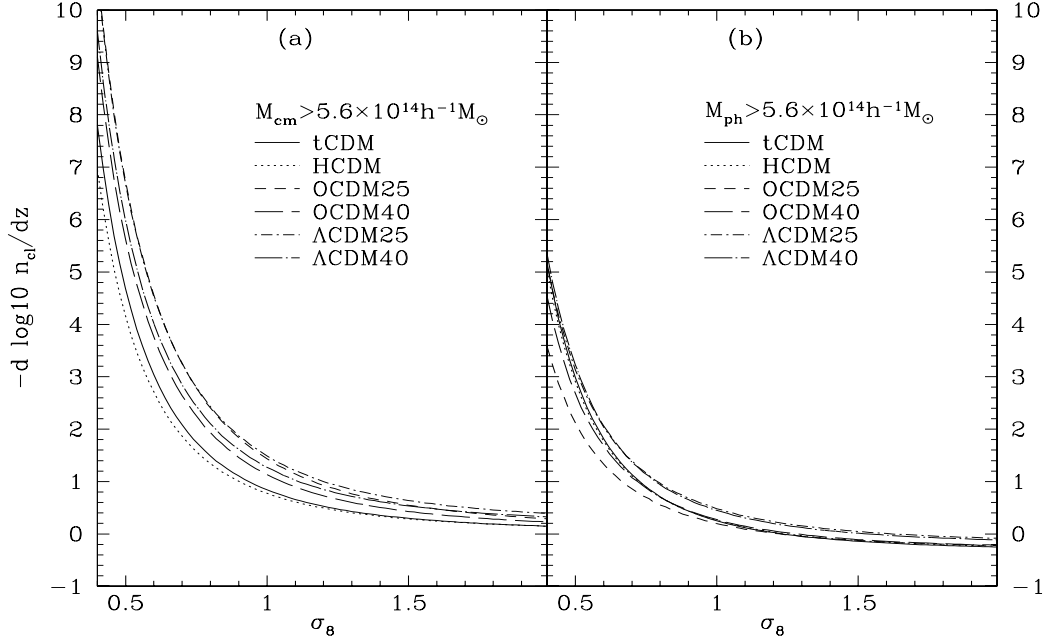
FIG. 7.— Panel (a) shows the number of clusters with mass $\geq 5.6 \times 10^{14} h^{-1} M_{\odot}$ within a fixed *proper* radius of $1.5 h^{-1} \text{Mpc}$, and panel (b) shows the evolution of the number of clusters with mass $\geq 7.9 \times 10^{14} h^{-1} M_{\odot}$ within a fixed *proper* radius of $1.5 h^{-1} \text{Mpc}$. The quantity in the vertical axis is the number of clusters per unit redshift per steradian. Shown as symbols are the observations with 2σ errorbars (Carlberg et al. 1997, C97; Luppino & Gioia 1995, LG95).

TABLE 2
NUMBER OF HIGH REDSHIFT X-RAY CLUSTERS^a IN SIX MODELS

Model	(5.0,7.0)keV $z > 0.5$	(5.0,7.0)keV $z > 1.0$	(5.0,7.0)keV $z > 2.0$
tCDM	(71, 2.2)	(1.3, 0.01)	(0.0, 0.0)
HCDM	(24, 1.3)	(0.19, 0.0028)	(0.0, 0.0)
OCDM25	(14902, 1374)	(10591, 798)	(3232, 139)
OCDM40	(3323, 273)	(1314, 70)	(75, 1.4)
ACDM25	(3217, 369)	(1005, 72)	(16, 0.30)
ACDM40	(1270, 112)	(203, 9.1)	(0.56, 0.0040)

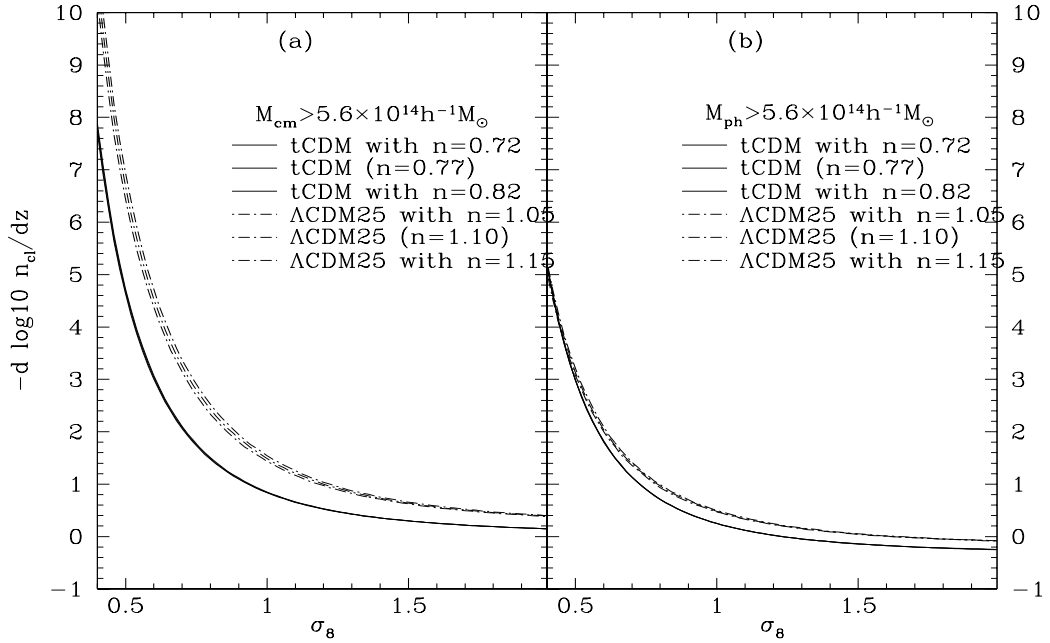
^afor a sky coverage of π steradian

Figure 8a



(8a)

Figure 8b



(8b)

FIG. 8.— (8a) shows the evolution rate of cluster number density as a function of the amplitude of the power spectrum (σ_8) for the six models (Table 1). Panels (a,b) of Figure (8a) show the evolution rate of number density for clusters whose mass ($=5.6 \times 10^{14} h^{-1} M_{\odot}$) is defined within a comoving Abell radius and within a physical Abell radius, respectively. (8b) shows the dependence of the evolution rate on power index n by varying n for tCDM and Λ CDM25.

ent σ_8 within a same model. Next, we select two models (tCDM and Λ CDM25) and let the power index n vary within the allowable ranges to test the dependence of \mathcal{E} on n . The results are shown in Figure 8b, from which we can easily draw the conclusion that the dependence of the evolution rate on n is very weak.

We conclude that the dramatic differences in the evolution rates between the different models are *almost entirely caused by the differences in σ_8* between the models, which results from the requirement that each model has to fit the cluster abundance at $z = 0$. *The apparent dependence of the evolution rates on Ω_0/Λ_0 is dictated by the strong dependence of cluster abundance on σ_8 through the $\sigma_8 - \Omega_0$ relation* (equation 36 of C98). This conclusion is in good agreement with that of Fan et al. (1998), who use the Press-Schechter method.

3.4. Gravitational Lensing by Clusters of Galaxies

Clusters of galaxies are so massive that they ubiquitously cause noticeable distortions of images of background sources even in their outskirts ($\sim 1 h^{-1}\text{Mpc}$) (Tyson, Valdes, & Wenk 1990; Miralda-Escudé 1991; Kaiser & Squires 1993). The central regions of rich clusters are often capable of producing more spectacular events such as large splitting, multiple images (of background quasars) or giant arcs (of background galaxies) (e.g., Le Fevre et al. 1994; Edge et al. 1994; Smail et al. 1996). These extreme gravitational lensing events are rare because the cross section for such events is small; usually only the central region of size of order several kiloparsecs in a very rich cluster is capable of producing giant arcs or multiple splittings of size of arcseconds and larger, compared to the usual notion of the size of a cluster ($\sim 1\text{Mpc}$) or even the size of the X-ray core ($\sim 100\text{kpc}$) of a cluster. Consequently, the frequency of such events is extremely sensitive to abundance of a very small population of very rich clusters at intermediate redshifts ($\sim 0.3 - 2.0$), where lensing is optimal.

Narayan & White (1998) compare strong lensing events in various models (pre-COBE) with observations combining Press-Schechter method with the singular isothermal sphere assumption. Cen et al. (1994) and Wambsgans et al. (1995) use detailed N-body simulations to compute the lensing statistics, focusing on intermediate splittings (a few arcseconds). Here we compute the frequency of very large splitting or giant arc events ($\sim \text{arcminute}$). We approximate each cluster as a singular isothermal sphere (SIS; Turner, Ostriker & Gott 1984, TOG henceforth) with the one-dimensional velocity dispersion determined by the mass within the comoving Abell radius:

$$\sigma_{||}^2 = \frac{GM_A(1+z_L)}{2r_A}, \quad (3)$$

where G is the gravitational constant, and z_L is the redshift of the (lens) cluster in question. For a SIS the bending angle, θ_0 , conveniently independent of impact parameter, is (TOG)

$$\theta_0 = 4\pi\left(\frac{\sigma_{||}}{c}\right)^2, \quad (4)$$

where c is the speed of light. The size of the arc due to such a lens will be approximated as the diameter of the Einstein ring as:

$$\beta = \frac{2\theta_0 D_{LS}}{D_S}, \quad (5)$$

where D_{LS} and D_S are the (comoving) angular diameter distance between the lens (cluster) and the source, and between observer and the source, respectively. The (comoving) angular diameter distances are dependent upon the geometry of a world model [$D_{LS} = D(\chi_S - \chi_L)$ and $D_S(\chi_S)$] as:

$$D(\chi) = \begin{cases} a_0\chi & \text{for flat universe } (\Omega_0 + \Lambda_0 = 1) \\ a_0 \sin(\chi) & \text{for close universe } (\Omega_0 + \Lambda_0 > 1) \\ a_0 \sinh(\chi) & \text{for open universe } (\Omega_0 + \Lambda_0 < 1) \end{cases} \quad (6)$$

Here, a_0 is a dimensional scale factor defined below; χ is the dimensionless comoving distance to the object in question at z , which can be expressed for an arbitrary universe (Refsdal, Stabell & de Lange 1967; Gott, Park & Lee 1989) as

$$\chi(z) = \sqrt{|3\sigma_0 - q_0 - 1|} \int_0^z Z(u)du, \quad (7)$$

where $Z(u) = [1 + 2(q_0 + 1)u + (q_0 + 1 + 3\sigma_0)u^2 + 2\sigma_0 u^3]^{-1/2}$. Here $\sigma_0 = \Omega_0/2$ and q_0 is the deceleration parameter, which is $q_0 = \Omega_0/2$ for $\Lambda_0 = 0$ and $q_0 = 3\Omega_0/2 - 1$ for $\Omega_0 + \Lambda_0 = 1$. The dimensional scale factor a_0 is $a_0 = \frac{c}{H_0\sqrt{|3\sigma_0 - q_0 - 1|}}$, where H_0 is the Hubble constant.

The dimensional comoving distance of an object at z is

$$r_{cm}(z) = a_0\chi(z). \quad (8)$$

Combining equations 3,4,5, we obtain an expression for the required cluster mass M_A in order to produce an arc of size β as

$$M_A(\beta) = \frac{\beta c^2 r_A}{4\pi G(1+z_L)} \frac{D_S}{D_{LS}}. \quad (9)$$

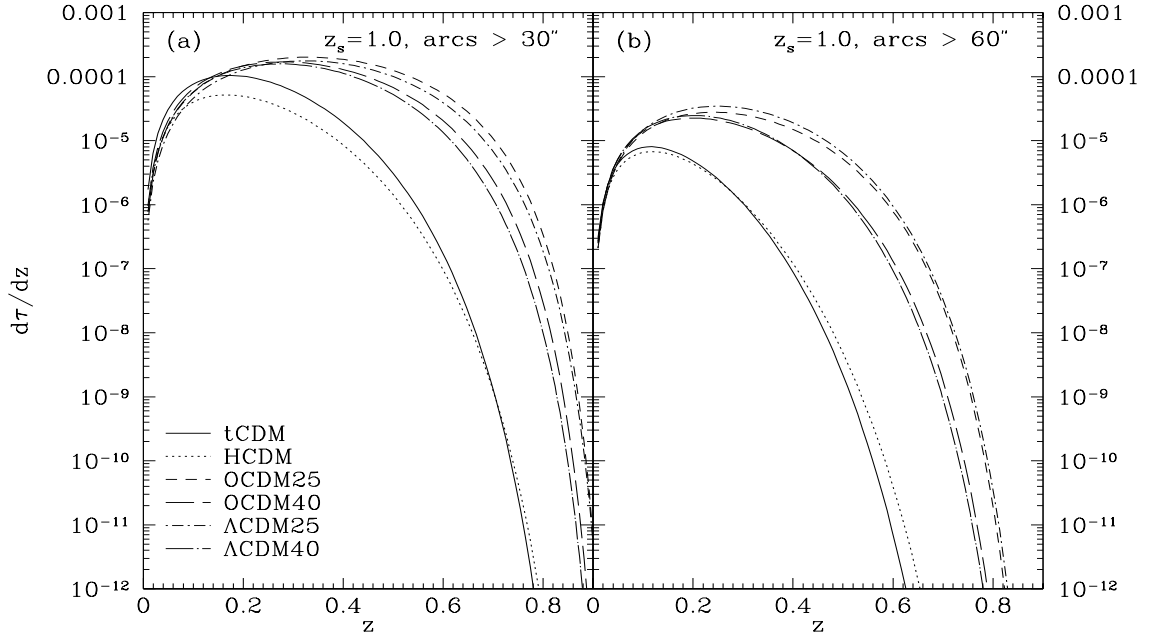
We can then compute the optical depth per unit redshift for forming arcs of size $> \beta$, as a function of redshift:

$$\frac{d\tau}{dz} = \pi\beta^2 \frac{dN_{cl}}{dz}, \quad (10)$$

where $\frac{dN_{cl}}{dz}$ is the number of clusters with mass $> M_A(\beta)$ (equation 9) per unit steradian per unit redshift, computed using GPM (C98).

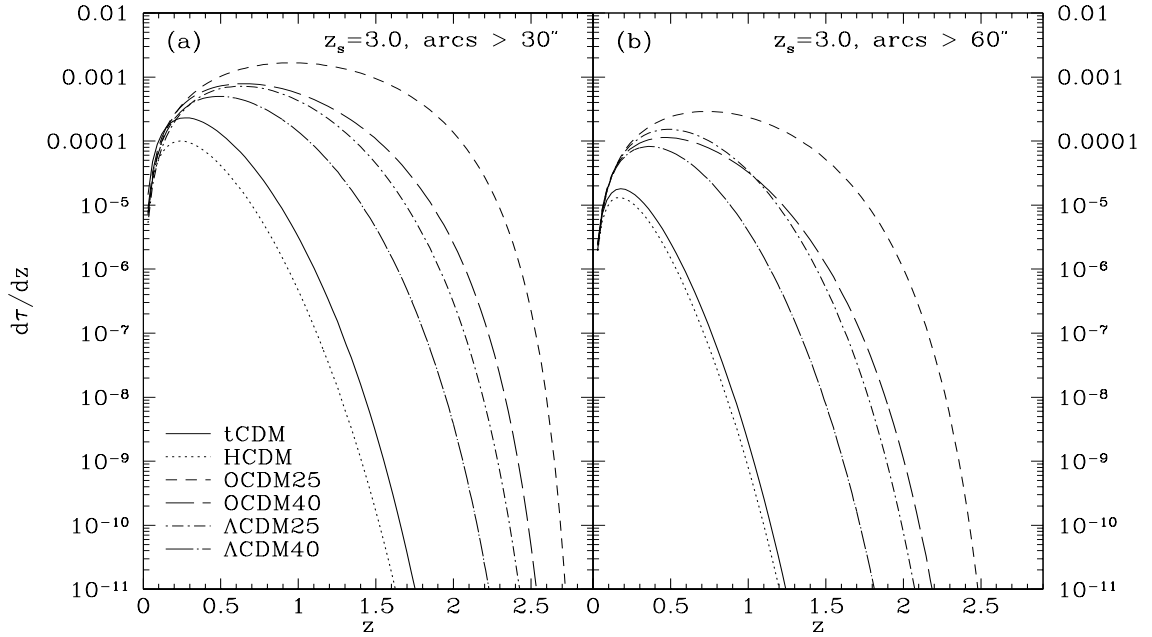
Figures (9a,b) show the (differential) gravitational lensing probability (i.e, differential optical depth) per unit redshift as a function of redshift for arcs or splittings greater than $30''$ and $60''$ for sources at $z_s = 1$ and $z_s = 3$, respectively. In accord with the evolution of cluster abundance as shown in Figures (5,6,7), the $\Omega_0 = 1$ models (tCDM, HCDM) have the lowest optical depths due to the rapid decrease in the number of rich cluster towards high redshift. The lowest Ω_0 models (OCDM25, Λ CDM25) have the highest optical depths. However, the difference between OCDM25 (open $\Omega_0 = 0.25$) and Λ CDM25 (flat $\Omega_0 = 0.25$) (similarly between OCDM40 and Λ CDM40) is more subtle: for sources at $z_s = 1$ Λ CDM25 has a somewhat higher optical depth than OCDM25 because the prolonged path length due to the cosmological constant in Λ CDM25 plays a significant role while the evolution rate of cluster abundance in the two models are comparable out to redshift ~ 0.5 ; but for sources at $z_s = 3$ OCDM25

Figure 9a



(9a)

Figure 9b



(9b)

FIG. 9.— The differential gravitational lensing probability (i.e., differential optical depth) per unit redshift as a function of redshift for arcs or splitting angles of multiple image events with sizes greater than $30''$ and $60''$ for sources at $z = 1$ (9a) and $z = 3$ (9b), respectively.

has a significantly higher optical depth than Λ CDM25 because the much lower rate of cluster abundance evolution in OCDM25 dominates over other factors.

The assumption of SIS is admittedly approximate, but used because of its analytical simplicity and because of its astrophysical relevance as used in many statistical studies (e.g., Tyson 1983; TOG; Narayan & White 1988; Fukugita & Turner 1991; Mao 1991). A perhaps more realistic profile is NFW profile (Navarro et al. 1996), which goes as r^{-1} in the center and as r^{-3} in the outskirt. Which profile, NFW or SIS, is more efficient for lensing depends on the core radius of clusters. If the core radius is sufficiently small, the NFW profile could be more efficient than a SIS profile, for a given cluster mass within a larger, given radius (Maoz et al. 1997). On the other hand, if the SIS assumption overestimates the strong lensing probability, this would diminish the already very small lensing optical depth in the high Ω_0 models further (the reductions in model with higher optical depths are smaller), widening the difference between models. Given the simplicity of our treatment, we choose to focus on the gross frequency of large gravitational arcs or large splitting multiple images, which are relatively robust, *not on the details such as length-to-width ratio of arcs*. The latter may sensitively depend on the small scale structures in the clusters such as core radius, inner density slope and substructure (see Bartelmann et al. 1997 for an excellent study on arcs of smaller sizes). The lack of or inadequate treatment of galaxy formation and inaccuracy in the small scale density distributions (even with very large, pure N-body calculations currently available) do not yet permit a sufficiently accurate characterization of lens potentials on small scales.

Clearly, the gravitational lensing optical depths of large arcs (or large splitting images) for different models deviate rapidly from one another towards high redshift. We argue that the errors introduced by our approximate method are likely to be substantially smaller than the difference between the models at moderate-to-high redshift. Detection of even a small sample (or non-detection) of such large lenses at redshift > 1.0 and/or a large sample of high redshift sources with such large arcs will provide a useful constraint on the models. Systematic surveys for large-image separation lensed quasars (Maoz et al. 1997) or arcs are beginning to provide useful statistical samples, and larger data sets such as from SDSS will be extremely powerful in constraining cosmological models. With the data set of 10^6 quasars from SDSS (assuming to be at $z_s = 3$ for this simple illustration), we expect to see (inferred from panel a of Figure 9b) (1900 ± 44 , 710 ± 27 , 570 ± 24 , 330 ± 18 , 100 ± 10 , 39 ± 6) multiple-image quasars with image separation $\geq 30''$ in (OCDM25, OCDM40, Λ CDM25, Λ CDM40, tCDM, HCDM), respectively (where the uncertainties are 1σ Poissonian). This would allow an unambiguous test of these six models. More likely, it would put a constraint on Ω_0 with $\Delta\Omega_0 \sim 0.01$ if the universe is open or $\Delta\Omega_0 \sim 0.03$ if the universe is flat. A more stringent test can be obtained if one also has the redshift distribution of the lenses. One expect to see (200.0, 4.0, 0.5, 0.005, 0.0, 0.0) lenses at $z \geq 2$ in (OCDM25, OCDM40, Λ CDM25, Λ CDM40, tCDM, HCDM), respectively, that produce arcs or splittings of size $\geq 30''$. We see that the differences between models in this measure are even more dramatic.

3.5. Ly α Forest

The abundant low column density Ly α forest lines in quasar absorption lines provide a precise and unbiased tracing of the distributions of neutral hydrogen, in a variety of environments, up to the highest redshift where quasars are observed to exist (e.g., Rauch et al. 1992; Schneider et al. 1993; Hu et al. 1995; Tytler et al. 1995; Lanzetta et al. 1995a; Bahcall et al. 1996). Until very recently, models of quasar absorption systems were *post hoc*. Successfully putting the formation and evolution of Ly α clouds into a cosmological context, computed *ab initio* from standard cosmological initial conditions (Cen et al. 1994; Zhang et al. 1995; Hernquist et al. 1996; Miralda-Escudé et al. 1996, MCOR hereafter; Bond & Wadsley 1997), has set forth a brand new way to study these objects. The surprisingly good agreement between simulations and observations in terms of matching the distributions of line width parameter b and column density, among other quantities, clearly demonstrates that the basic cosmological origin for Ly α clouds is no longer questionable.

It is to distinguish between competing cosmological models that interests us most here. We attempt to check illustratively if Ly α forest may be used to test cosmological models. We will only examine models at $z = 2$, where good observational data are available. Figure 10 shows the power spectra (panel a) and the rms density fluctuations (panel b), both in real space and computed using linear theory, at the relevant scales ($k \sim 1.0 - 30.0h/\text{Mpc}$ and $H(z)r_{TH} \sim 10.0 - 300.0\text{km/s}$) at $z = 2$. In order for the models to be shown and compared on a common, relevant physical scale, the Hubble velocity instead of proper (or co-moving) physical distance is shown in the x-axis in panel (b). Also shown as a cross-shaded region is the observational constraint adapted from Rauch et al. (1997). The adopted observational constraint is based on the range of the fluctuation amplitudes on the relevant scales spanned by the two models (SCDM and Λ CDM; Figure 8 of Rauch et al. 1997) examined by Rauch et al. (1997), which fit the observations well and provide a useful indication in the needed power on the relevant scales. The plotted vertical range of the shaded box is three times the range between SCDM and Λ CDM in Rauch et al. (1997), centered on the mean amplitude (at each x-axis value) averaged over the SCDM and Λ CDM models.

The disparity of powers between the models on these scales relevant to the formation of Ly α clouds is rather striking. The very slow growth of perturbations at low density open models is clearly manifested: OCDM25 (open $\Omega_0 = 0.25$) has distinctly more power on all the shown scales than other models, while HCDM has power at $k = 30h/\text{Mpc}$ lower than that of OCDM25 by almost two orders of magnitude. These differences should result in distinctly different populations of Ly α forest lines and flux distributions. We expect that the overall flux distributions (Rauch et al. 1997) of the models will be different, even with the liberty to adjust the ionization rate to fit the observed mean flux decrement (Zuo & Lu 1993; Press, Rybicki, & Schneider 1993). In particular, the low flux end of the 1-point flux distribution will be dramatically different between the models (Cen 1997a). Since the amount of observational data available (and accumulating) on Ly α forest lines are very large, measures based on flux distri-

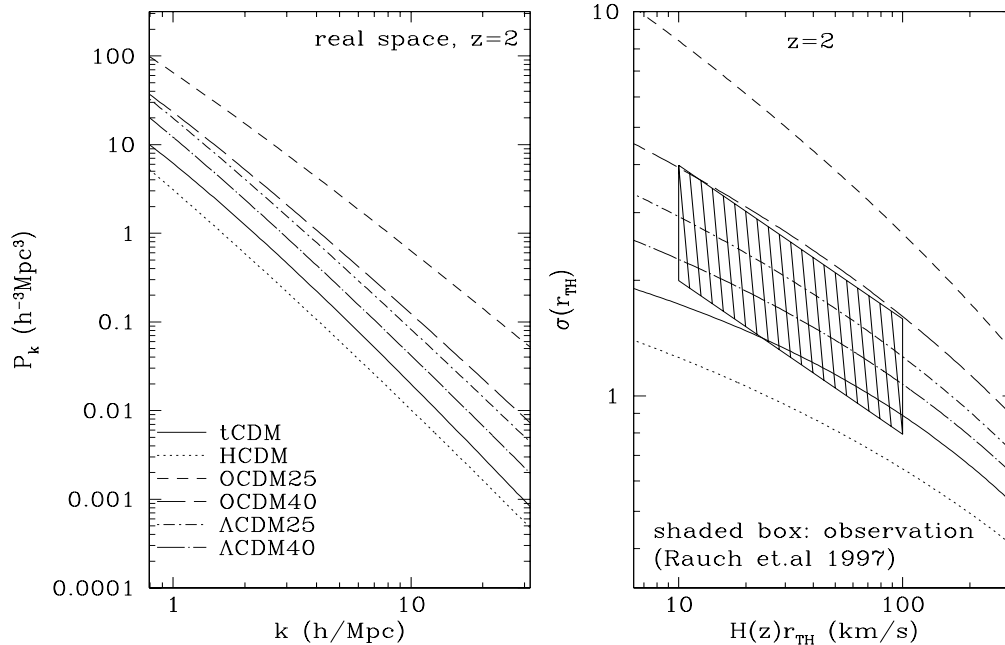


FIG. 10.— The power spectra (panel a) and the rms density fluctuations (panel b), both in real space, at the relevant scales ($k \sim 1.0 - 30.0h/\text{Mpc}$ and $H(z)r_{\text{TH}} \sim 10.0 - 300.0\text{km/s}$) at $z = 2$, computed using linear theory. Also shown as a cross-hatched region is the observational constraint adapted from Rauch et al. (1997). In panel (b) the x-axis is in km/s, obtained by multiplying the physical scale (r_{TH}) by the Hubble constant at $z = 2$, $H(z)$.

butions (MCOR; Cen 1997a; Miralda-Escudé et al. 1997) may enable tests of models with high statistical significance. Preliminary comparisons between models and observations using the one-point flux distribution probability function (Rauch et al. 1997) seem to most favor the two Λ based models (Λ CDM25 and Λ CDM40), but disfavor HCDM and OCDM25 in the opposite sense that HCDM has too little power and OCDM25 has too much power on the relevant scales. tCDM and OCDM40 appear to be marginally consistent.

Definitive theoretical predictions of all the models and comparisons between models and observations await detailed modeling using cosmological hydrodynamic simulations suitable to study the formation of Ly α clouds (Cen et al. 1994; Zhang et al. 1995).

3.6. Damped Ly α Systems

The high end of the Ly α clouds is the damped Ly α systems, which are thought to be progenitors of large disk galaxies (Wolfe 1995). Damped Ly α systems are much rarer than the common Ly α forest lines by approximately two orders of magnitude, analogous to relative abundances between galaxies and clusters of galaxies at present time. In this sense damped Ly α systems probe the tail of the density distribution on $\sim 1h^{-1}\text{Mpc}$ scale at high redshift, whereas present clusters of galaxies probe the tail of the density distribution on $\sim 10h^{-1}\text{Mpc}$ scale.

Prochaska & Wolfe (1997) find that the only model among tested that matches the observed kinematics of damped Ly α systems is a thick fast rotating disk of rotation speed of $> 180\text{km/s}$ (99% confidence level) with the most likely rotation velocity being 225km/s . This thus seems to provide an additional piece of evidence that damped Ly α systems may be the progenitors of present

large disk galaxies. We adopt the observed lower bound on the rotation speed of 180km/s to compare with models. Figure 11 shows the density of collapsed baryons in systems with rotation velocity (equation 18 of C98) greater than 180km/s as a function of redshift, computed using GPM (C98). The observations are from Lanzetta et al. (1995b, L95 henceforth) and in Figure 11) and Storrie-Lombardi et al. (1996, S96 henceforth) with 1σ errorbars. The errorbars are those adopted in S96 for both sets of observations. A small complication arises from the fact that the observations are tabulated only for models with $q_0 = 0$ and $q_0 = 0.5$ [Table 1 of S96]. We compute the observed values for other models by linear interpolating $h\Omega_g$ between the two tabulated models using weighting of the inverse of the Hubble constant at each redshift bin. This is justified since the absorption distance interval is inversely proportional to the Hubble constant at the redshift in question: $\Delta X = (1+z)^2 [H_0/H(z)]$ (Bahcall & Peebles 1969), where $H(z) = H_0 \sqrt{\Omega_0(1+z)^3 + (1-\Omega_0-\Lambda_0)(1+z)^2 + \Lambda_0}$ (Peebles 1993). It is, however, still approximate due to non-uniform distributions of absorption redshift paths within each bin and finite sizes of the redshift bins.

Without running detailed hydrodynamic simulations we wish only to *conservatively* assume that all the baryons (which is proportional to the mass with a fixed ratio equal to the global ratio) that collapse into these systems are in neutral form. This is conservative in the sense that it is an upper bound on Ω_g , since some amount of hydrogen may be in other forms such as ionized or molecular form. Bearing in mind that the computed quantity is an upper bound, we see that HCDM is inconsistent with observations at a high confidence level, in agreement with

Figure 11

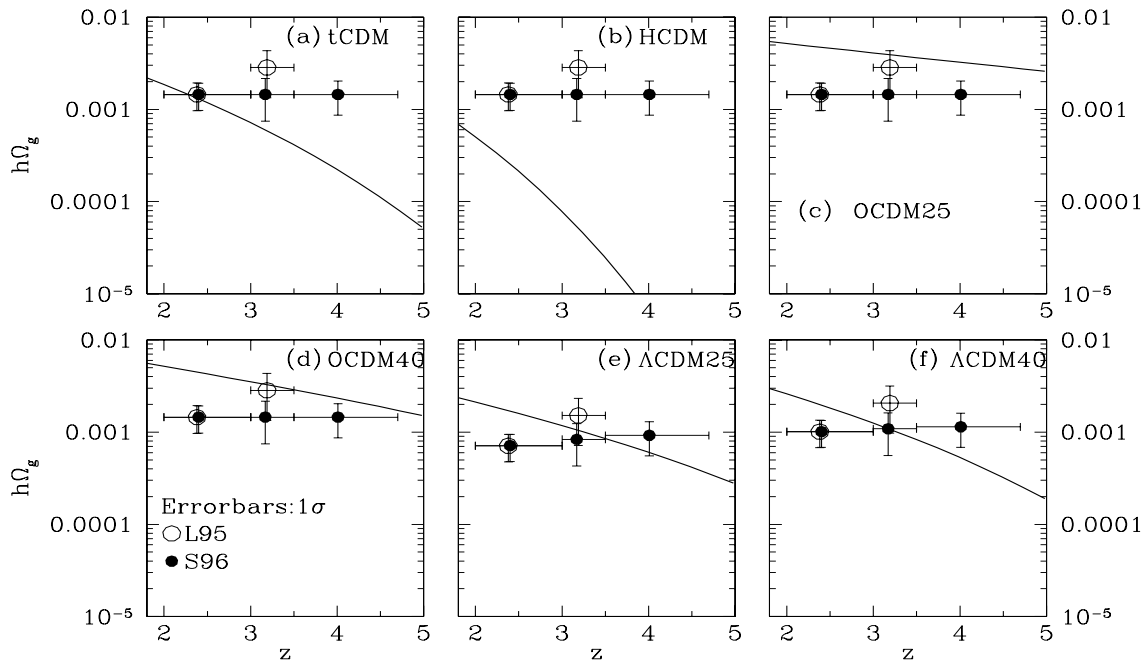


FIG. 11.— The gas density of collapsed baryons in systems with rotation speed of > 180 km/s, as a function of redshift for six models. The observations are from Lanzetta et al. (1995) and Storrie-Lombardi et al. (1996) with 1σ errorbars.

the conclusion drawn by Ma et al. (1997) for a comparable model, and consistent with previous analyses (Subramanian & Padmanabhan 1994; Kauffmann & Charlot 1994; Mo & Miralda-Escudé 1994; Klypin et al. 1995), which use an HCDM model with a somewhat larger fraction of mass being in hot neutrinos ($\Omega_h = 0.3$). Note that the newer observation with significantly absorption path length in S96 than in L95 has revised and significantly lowered the point at $z = 3.19$. But the basic conclusions previously reached by other authors with regard to HCDM model remain valid. All the other models are consistent with observations with perhaps the exception of OCDM25 (open $\Omega_0 = 0.25$), which appears to have overproduced the neutral hydrogen gas in these systems. But we recall that photoionization and other heating sources could significantly reduce the neutral hydrogen fraction in these systems. Therefore, OCDM25 cannot be ruled out yet without more detailed calculations.

3.7. High Redshift Galaxies

Recently, observations of high redshift galaxies have made major break-throughs by using an innovative technique to systematically and efficiently search for them (Pettini et al. 1997; Steidel et al. 1998, S98 henceforth). Interesting discoveries have already been made with a relatively small sample of such galaxies (~ 200). S98 find a large concentration of galaxies in redshift space near redshift three in a field of size about 9×15 arcmin². The concentration is so large for $z \sim 3$ that S98 are able to draw some interesting implications for cosmological models and galaxy formation. We will use a somewhat different method to conservatively assess the implications of such high redshift galaxy observations for models. In particular, we will try to address how likely such a large con-

centration of galaxies will occur in various models.

We first note that Pettini et al. (1997) give a selection function (in redshift) of their observations simply by fitting the observed distribution of galaxies in the redshift range $z = 2 - 4$. This approach would be valid, *if the distribution of galaxies in redshift in the range of interest is constant*. In general, the density of galaxies needs not be constant in redshift. Without *a priori* determined selection function, we simply use a Gaussian selection function, $\exp(-(z - \bar{z})^2 / 2\sigma_{SF}^2)$, where the mean \bar{z} is chosen to be 3.07 to maximize the selection function value at the peak of the observed galaxy concentration ($z = 3.05 - 3.09$) (this is conservative in the sense that it maximize a model's ability to match such a large concentration), and $\sigma_{SF} = 0.35$ will be used. Such a choice of selection function seems appropriate for the observational technique used which optimizes detection at $z \sim 3$ (Pettini 1997, private communications), and should be adequate for our purpose in the sense that our results do not sensitively depend on the choices of \bar{z} and σ within reasonable ranges. By the way, this chosen selection window function turns out to be quite close to what is empirically obtained from observations (Figure 2 of Pettini et al. 1997).

Figure 12 shows the distribution of galaxies (halos) for each model without (dotted curve) and with (solid curve) the selection function. For each model we allow ourselves the liberty to adjust the threshold of the virial mass of the halos until the number of galaxies in the redshift range $z = 2 - 4$ matches what is observed. S98 find that 180 galaxies satisfy their color selection criteria and about 5% of them turn out to be stars in the field SSA22 of size $8'.74 \times 17'.64$. We will simply assume that there are $181 \times (1 - 0.05) = 172$ observed galaxies in the range $z = 2 - 4$, to which our models are normalized. We

Figure 12

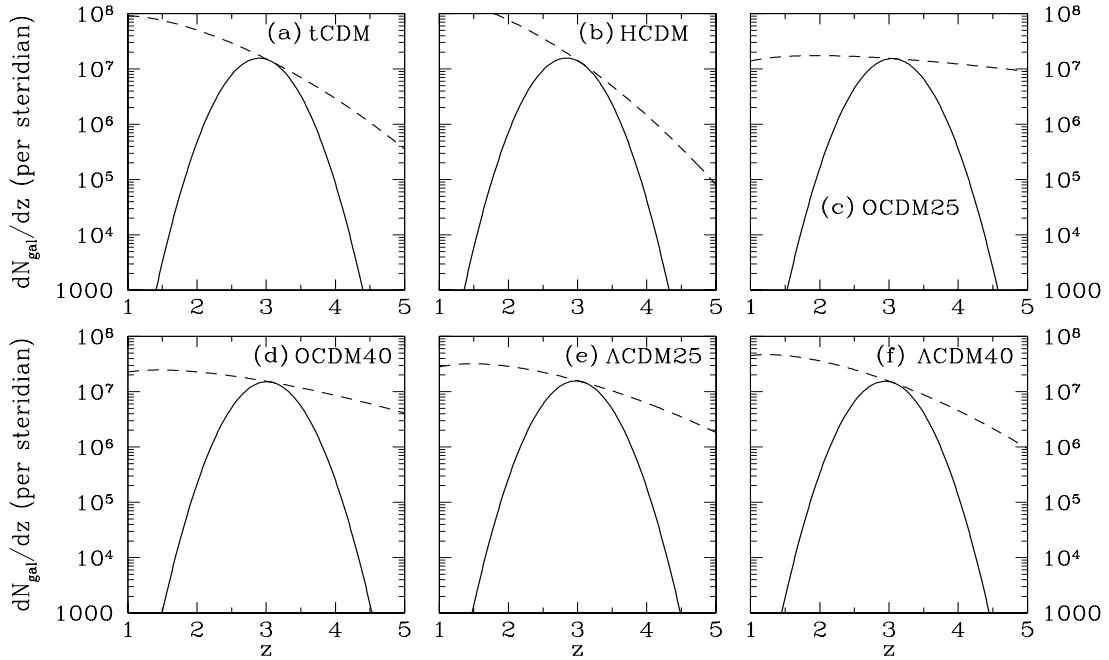


FIG. 12.— The number of galaxies (halos) per steradian per unit redshift without (dashed curves) and with (solid curves) the observational selection function (see text for the definition of the observational selection function). The number of galaxies (with the observational selection function) in each model is normalized to what is observed in the redshift range $z = 2 - 4$ by Steidel et al. (1997).

use GPM (C98) to compute the abundance of such halos. Normalizing the number density of galaxies (halos) in each model requires to impose quite different velocity dispersion threshold (the velocity dispersion-mass relation is governed by equation 18 and the virial radius-mass relation by equation 12 of C98) for the virialized halos as tabulated in Table 3. Preliminary observational evidence indicates that the high redshift galaxies have velocity dispersions in the range $\sigma_{||} = 180 - 320\text{km/s}$ (Steidel et al. 1996). We thus see that the current observed range in $\sigma_{||}$ has already become interesting in terms of imposing a constraint on the models. If future observations can significantly narrow the range, then the combination of $\sigma_{||}$ and density may be quite powerful to discriminate between models. We further note the volume-limited redshift distributions of galaxies (solid curves in Figure 12) are quite different in different models. So a direct observation of this (without narrow observational selection window functions) in a sufficiently large range in redshift, perhaps by a combination of several observational techniques/passbands, will be very important.

The field of view of size $8'.74 \times 17'.64$ corresponds to different sizes (L_x, L_y) in comoving length units for different models, so does the redshift bin size ($\Delta z = 0.04; L_z$), all of which are listed in Table 3 along with some other relevant quantities. We compute the rms fluctuations of total mass in a box of comoving size $L_x \times L_y \times L_z$ for each model at $z = 3$, $\sigma_{m,box}$, using the following formula in Fourier space:

$$\sigma_{m,box}^2 = \frac{1}{(2\pi)^3} \int_0^\infty \int_0^\infty \int_0^\infty \frac{[\sin(0.5L_x k_x)/(0.5L_x k_x)]^2}{[\sin(0.5L_y k_y)/(0.5L_y k_y)]^2} \frac{[\sin(0.5L_z k_z)/(0.5L_z k_z)]^2}{[\sin(0.5L_z k_z)/(0.5L_z k_z)]^2} dk_x dk_y dk_z,$$

$$P_k dk_x dk_y dk_z, \quad (11)$$

where P_k is the power spectrum at $z = 3$. Note that we have assumed that *there is no peculiar velocity distortion along the line of sight*, when computing L_z . This assumption is conservative in the sense that the actual extent in real space would be larger than the indicated L_x , if the linear compression along the line of sight for an overdense region is more important than the finger-of-god effect due to the internal velocity dispersion of the collapsed object. We have the following reason to believe that this is the case. Given the observational evidence that such peaks are fairly common (S98), it is highly unlikely that they are *very rich* clusters of galaxies, thus internal velocity dispersion is unlikely to be important on the indicated scales of L_z . To be somewhat more quantitative, a velocity dispersion of 1000km/s corresponds to $5h^{-1}\text{Mpc}$ comoving at $z = 3$ in an $\Omega_0 = 1$ model, significantly smaller than $L_z = 15h^{-1}\text{Mpc}$ in the same model.

Let us now compute the bias factor of the halos at $z = 3$ using the method similar to that used to compute the correlation of clusters (equation 28 of C98): $b_{halo} \equiv \frac{\langle \tilde{v} \rangle}{\sigma_0} + 1$, which is listed in Table 3. $\langle \tilde{v} \rangle$ is computed using equation 29 of C98 and σ_0 is the rms fluctuation, both computed for a density field at $z = 3$ smoothed by a Gaussian window chosen to produce the correct number density of halos (C98). We see that peaks are moderately biased over mass in low density models but strongly biased in $\Omega_0 = 1$ models, in agreement with the conclusion drawn by S98.

If a linear bias of halos over mass on the relevant large scales (i.e., on the box scale) exists, as supported by detailed galaxy formation simulations (Cen & Ostriker 1992b; Blanton et al. 1998) and analytical arguments (Gra-

TABLE 3
HIGH REDSHIFT GALAXIES IN SIX MODELS

Model	L_x ($h^{-1}\text{Mpc}$)	L_y ($h^{-1}\text{Mpc}$)	L_z ($h^{-1}\text{Mpc}$)	σ_{\parallel} (km/s)	$\sigma_{m,box}$	b_{halo}
tCDM	7.63	15.4	15.0	165	0.138	4.82
HCDM	7.63	15.4	15.0	115	0.131	6.38
OCDM25	10.8	21.8	22.7	243	0.320	1.90
OCDM40	9.65	19.5	20.2	224	0.239	2.71
Λ CDM25	11.9	24.1	29.3	202	0.207	3.30
Λ CDM40	10.4	20.9	23.4	185	0.178	3.92

Figure 13

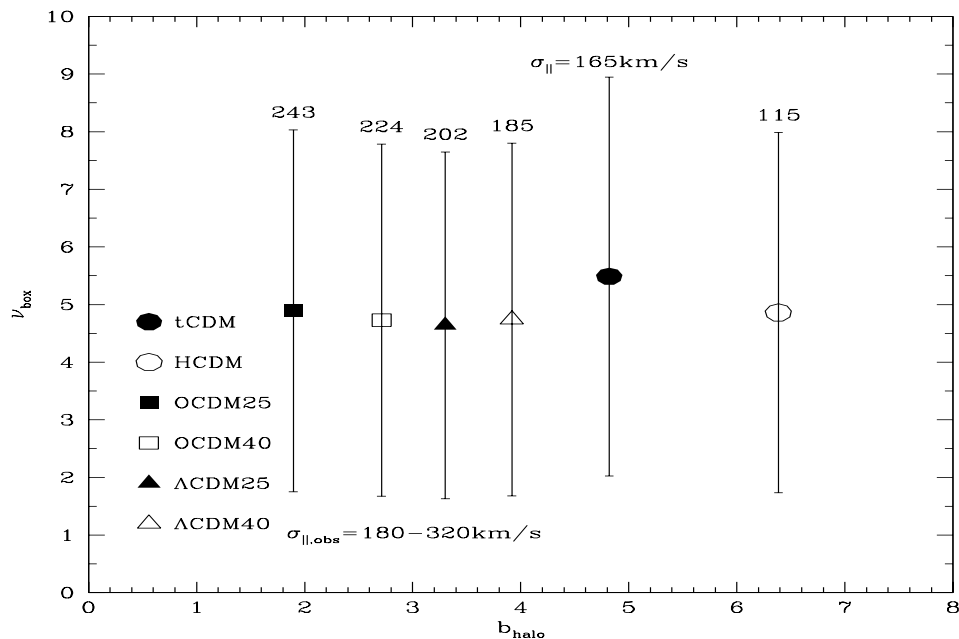


FIG. 13.— Peak height of the box ($\nu_{halo,box}$) against the bias of galaxies over the matter on the box (b_{halo}) is plotted for each model. The range in vertical axis for each model is (2σ) statistical fluctuations due to small number of galaxies in the observed galaxy peak. Also shown above each vertical errorbar is the velocity dispersion threshold of halos in each model, along with the observed range shown near the bottom of the plot.

mann & Einasto 1992), one obtains

$$\sigma_{halo,box} = b_{halo}\sigma_{m,box}, \quad (12)$$

where $\sigma_{halo,box}$ is the rms fluctuations of halos in a box of comoving size $L_x \times L_y \times L_z$ at $z = 3$. We first compute the number of galaxies (without the selection function) in each model in the redshift range $z = 2.4 - 3.8$ consisting of 35 redshift bins each of size $\Delta z = 0.04$ (Steidel et al. 1998), $N_{2.4-3.8}$. Dividing $N_{2.4-3.8}$ by 35 gives the average number of galaxies in each redshift bin of size, \bar{N} . Since the total number of spectroscopically identified galaxies is only 78 in the redshift range $z = 2.4 - 3.8$, we need to compensate for the fraction of spectroscopically yet unidentified galaxies, which will be assumed here to have the same redshift distribution as the spectroscopically identified ones. This is accounted for by multiplying the relevant galaxy number by the ratio, $N_{2.4-3.8}/78$. Now, we can compute the height of the observed galaxy peak at $z = 3.07$ in terms of the rms fluctuations in the indicated box ($L_x \times L_y \times L_z$) in each model:

$$\nu_{box} = \frac{N_{peak}(N_{2.4-3.8}/78)/\bar{N}}{\sigma_{halo,box}} - 1, \quad (13)$$

where N_{peak} is the number of galaxies in the observed redshift peak near $z = 3$. There are 15 spectroscopically identified galaxies in the peak ($\Delta z = 3.05 - 3.09$) in the SSA22 field, which gives a 2σ upper and lower range of $N_{peak} = 15 \pm 8$ due to Poisson fluctuations.

Figure 13 shows ν_{box} as a function b_{halo} . The range in the vertical axis for each model is due to (2σ) Poisson statistical fluctuations of the small number of galaxies in the observed galaxy peak. Also shown above each vertical errorbar is the velocity dispersion threshold of halos in each model, along with the observed range shown near the bottom of the plot. Clearly, the vertical ranges are large. Hence, a larger sample of such events will be invaluable to dramatically shrinking the size of the errorbars. If such galaxy concentrations turn out to be as common as 2σ events in the real world, then all the models would have to be re-evaluated. The two $\Omega_0 = 1$ models (tCDM and HCDM) have one additional inconsistency with observations: they do not have enough massive halos to host galaxies with velocity dispersion as large as indicated by the preliminary observations.

It should be pointed out that the GPM method used here to compute the halo statistics ignores merger. But it may be argued that, in this case, this peak counting method may be more accurate than direct N-body simulations for precisely the reason that merger is ignored. Overmerging of galaxies (identified with halos) in N-body simulations is error-prone due to lack of realistic physics/sufficient resolution. In real world, although halos may still merge, most galaxies are likely to retain their separate identities (for example, a rich cluster like Coma contains hundreds of galaxies but might consist of only a handful of dark matter halos). This is, of course, not in conflict with some unavoidable processes occurring in the real world that may transform the morphologies of galaxies but do not produce direct merger, such as galaxy harassment (Moore et al. 1996). Thus, our treatment by ignoring merger may in fact be closer to truth than halos

identified in direct N-body simulations in terms of correctly counting galaxies. If halo merger is more important in objects such as the observed galaxy concentration in the real world, inclusion of some merger effects would exacerbate the problem, as merger would reduce the number of galaxies in high density region (as considered here) and reduce the bias of galaxies (in number) over mass in the models. Interestingly, our results, namely that the high redshift galaxies are highly biased over mass, are in broad agreement with results from N-body simulations (Bagla 1998; Jing & Suto 1998; Governato et al. 1998).

We note in passing that directly measuring the bias of galaxies over mass at high redshift will prove to be extremely difficult. The only *direct* measurement of the distribution of underlying mass has to come from direct mapping by gravitational lensing. But such a measurement, even if possible in principle, is very difficult. This situation is further worsened by the fact that matter at $z = 3$ does not make an optimal contribution to the lensing effect compared to matter at lower redshifts. There is, however, one possible, though somewhat less direct, measurement of the bias of galaxies over mass. It makes use of the fact that it is possible to select a population of Ly α clouds whose clustering strength is comparable to that of the underlying matter. Then, a comparison between the clustering of such Ly α clouds and the clustering of galaxies both at the same high redshift would yield a measurement of bias (of galaxies over matter). This technique has recently been proposed by Cen et al. (1998). But detailed computations of various models are needed in order to understand the relationship between matter and Ly α clouds in different models, before one can make self-consistent calibration to infer the clustering of mass from that of Ly α clouds.

3.8. Reionization of the Universe

To properly tackle this issue requires detailed hydrodynamic modeling with three-dimensional radiative transfer. Cosmological hydrodynamic simulations (Cen & Ostriker 1993a; Ostriker & Cen 1996; Gnedin & Ostriker 1997) as well as analytic analyses (Haiman & Loeb 1997) have demonstrated that the detailed picture of reionization of the universe depends on many uncertain parameters, including the properties of the ionizing sources, the clumpiness of the baryonic density field, the mean baryonic density, etc.

We want to address the following comparatively simpler question: When was the universe completely reionized? It is possible to obtain a relatively accurate result if one only wants to identify the epoch when the universe gets completely reionized (ignoring the detailed development of the reionization process). In this case one just needs to count the number of ionizing photons. When the number of ionizing photons emitted per hydrogen atom in one (hydrogen) recombination time is equal to one, the universe (with regard to hydrogen) is completely ionized. We now formulate this criterion quantitatively, assuming that the universe is reionized primarily by UV ionizing radiation from massive stars of early galaxies.

The Hubble time as a function of redshift is (Peebles 1993)

$$t_H(z) = t_0 [\Omega_0(1+z)^3 + (1 - \Omega_0 - \Lambda_0)(1+z)^2 + \Lambda_0]^{-1/2}, \quad (14)$$

where $t_0 = 9.78h^{-1}$ Gyr is the present Hubble time. The hydrogen recombination time is

$$t_{rec} = [1.16n_H\alpha(T)C^2]^{-1} = 2.0 \left(\frac{\Omega_b h^2}{0.0125} \right)^{-1} \left(\frac{1+z}{6} \right)^{-3} C^{-2}, \quad (15)$$

where 1.16 comes from the fact that the primordial gas has a (76%, 24%) (H, He) composition, $\alpha(T)$ is the hydrogen recombination coefficient and $C \equiv \sqrt{\langle \rho_b^2 \rangle / \langle \rho_b \rangle^2}$ is the gas clumping factor (we have ignored here the difference between total baryonic matter and ionized hydrogen assuming that hydrogen is ionized everywhere). For the second equality in equation 15 we assume $T = 1.5 \times 10^4$ K, giving $\alpha = 6.9 \times 10^{-13}$ cm³/sec (Cen 1992). Assuming that a fraction, ϵ_{UV} , of the rest mass energy of collapsed systems is converted into ionizing photons in a short time scale (i.e., star formation for the relevant massive stars is assumed to be almost instantaneous once a galaxy has collapsed), we can write down the equation, equating the number of ionizing photons emitted per hydrogen atom in a recombination time to unity, as:

$$\frac{\epsilon_{UV} m_p c^2}{h\nu_0} \frac{df_g}{dz} \frac{dz}{dt_H} t_{rec} = 1, \quad (16)$$

where df_g/dz is the fraction of total baryonic matter that has collapsed and condensed out to form galaxies per unit redshift, m_p is proton mass, c is the speed of light and $h\nu_0$ ($= 13.6$ eV) is the hydrogen ionization potential. Using equations (14,15) to expand equation (16), one finds

$$\frac{df_g}{dz} = 1.2 \times 10^{-9} h^{-1} \epsilon_{UV}^{-1} \left(\frac{\Omega_b h^2}{0.0125} \right) \left(\frac{1+z}{6} \right)^{1/2} C^2 \left[\Omega_0 + (1 - \Omega_0 - \Lambda_0)(1+z)^{-1} + \Lambda_0(1+z)^{-3} \right]^{-3/2} \left[\Omega_0 + \frac{2}{3}(1 - \Omega_0 - \Lambda_0)(1+z)^{-1} \right]. \quad (17)$$

The main uncertainties in this treatment include: the star formation history of the high redshift galaxy, the initial mass function (IMF) of the stars, and the fraction of UV ionizing photons that escape host galaxies and enter the inter-galactic medium (IGM), the clumpiness of the gas and complicated interplay between radiation self-shielding of dense, optically thick regions and absorption of UV photons by these regions. An accurate treatment of this problem awaits detailed galaxy formation simulations with a sufficiently realistic treatment of three-dimensional radiative transfer. The present study serves to illustrate the large differences between models with regard to the reionization epoch, which may survive detailed, more accurate simulations. In the present treatment all these various factors have been conveniently condensed into the single parameter ϵ_{UV} , being the fraction of the rest mass of stars that turn into ionizing UV photons escaping into the IGM. We will use $\epsilon_{UV} = (3 \pm 2) \times 10^{-5}$, which is lower than the values previously used (Gnedin & Ostriker 1997; Cen & Ostriker 1998) by approximately a factor of two. This factor of two is intended to account for the slight over-counting of the number of ionizing photons in equation 16, where all ionizing photons are treated to be at Lyman limit, in contrast to an Orion-like spectrum of a young stellar association (Scalo 1986). A clumping factor $C = 7.0$ is

used, which may be uncertain by a factor of a few, perhaps in the upward direction.

The required galaxy formation rate per unit redshift df_g/dz (equation 17) is shown as the cross-shaded bands in Figure 14, where the upper and lower limits are due to the uncertainty in ϵ_{UV} . The solid curves in Figure 14 show the fraction of matter in collapsed (virialized) systems per unit redshift with velocity dispersion greater than 35km/s (corresponding to virial temperature of $\sim 10^4$ Kelvin), as a function of redshift, that are assumed to emit the ionizing photons. Smaller systems are unlikely to be able to collapse due to the lack of efficient coolants at $T < 10^4$ K in the presence of significant photo-ionizing radiation field (Efstathiou 1992; Quinn, Katz, & Efstathiou 1996) or in the presence of feedback processes from young galaxies (Cen & Ostriker 1993a); molecular hydrogen could have served as an efficient coolant at the lower temperatures but they are likely to have been destroyed long before these sub-galactic size objects start to form (Ostriker & Gnedin 1996; Haiman, Rees, & Loeb 1997).

We see that different models predict quite different epochs of reionization of the universe, which are tabulated in Table 4 for the ease of comparison. It is noted that the exact epoch of reionization is quite insensitive to small variations of ϵ_{UV} or the degree of clumpiness of the medium, simply because it is during the rapidly rising part of the evolution of the collapse fraction when the reionization occurs. It is clear that observations to higher redshift would provide a powerful discriminator between models. For example, if the universe is observed to be transparent at $z > 5$, then HCDM will be inviable; if the universe is observed to be transparent at $z > 10$, the all but the open models will be ruled out.

While it is beyond the scope of current paper to conduct detailed calculations of the properties of high redshift objects around the reionization epoch in each model, we only briefly comment that near future observations by meter waves telescopes such as Giant Meterwave Radio Telescope (GMRT; Swarup 1984) and the Kilometer Square Array Interferometer (SKAI; Braun 1995) and the next generation infrared telescopes such as the Space Infrared Telescope Facility (SIRTF; Werner & Eisenhardt 1988) and Next Generation Space Telescope (NGST) will shed light on the properties of objects at the reionization epoch such as neutral hydrogen condensates (Scott & Rees 1990; Subramanian & Padmanabhan 1993; Madau, Meiksin, & Rees 1997) and ionizing sources (Haiman & Loeb 1997; Miralda-Escudé & Rees 1997). In addition, the differences in the reionization time thus in optical depth to CMB photon and in angular scales would leave different imprints on CMB at small angular scales.

3.9. CMB Experiments: MAP and PLANCK

Needless to say, future CMB experiments are likely to provide a very rich amount of information, that can be used in many aspects to constrain cosmological models as well as understanding astrophysical processes involved. However, cosmological parameters determined from CMB experiments alone are likely to display certain degeneracies (e.g., Efstathiou & Bond 1998). Other astronomical and cosmological phenomena discussed in the preceding sections are, in this sense, complementary to CMB observations. Here we choose to focus on one parameter, which

Figure 14

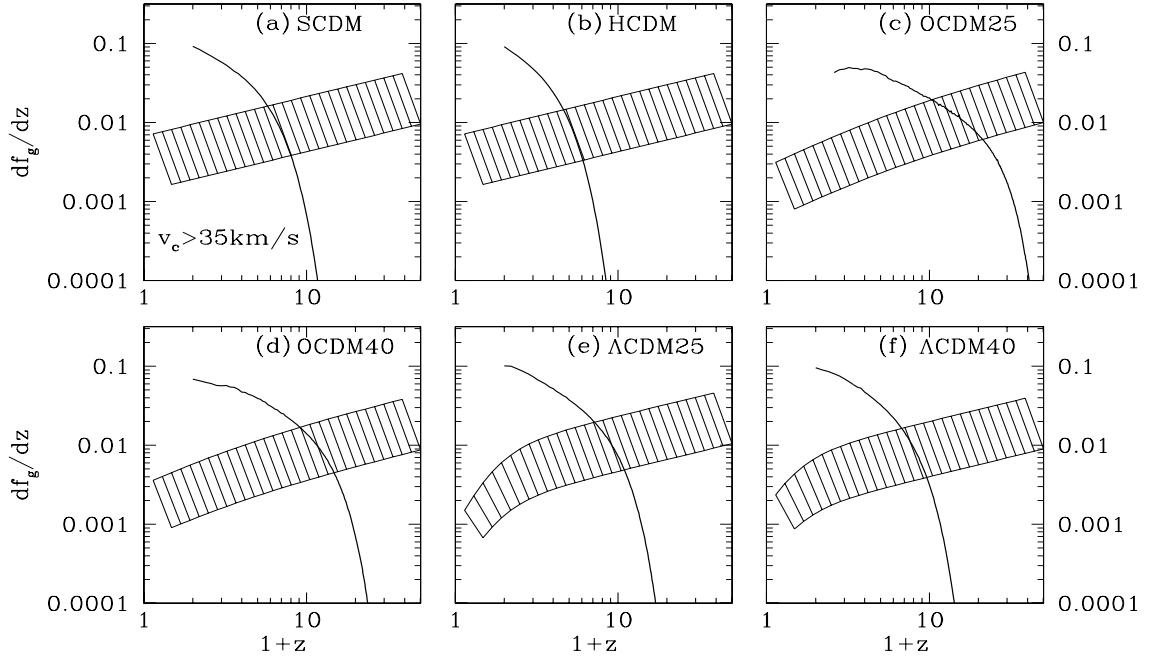


FIG. 14.— The fraction of matter formed per unit redshift in collapsed (virialized) systems with velocity dispersion greater than 35km/s (corresponding to virial temperature of $\sim 10^4$ Kelvin), as a function of redshift in six models. Each cross-shaded band indicates the required range with which enough UV photons are produced to completely reionize the entire universe.

TABLE 4
REIONIZATION EPOCHS IN SIX MODELS

Model	z_{rei}
tCDM	5.8 – 8.2
HCDM	3.7 – 5.6
OCDM25	28.0 – 36.0
OCDM40	13.0 – 20.0
Λ CDM25	10.0 – 13.0
Λ CDM40	7.7 – 10.0

Figure 15

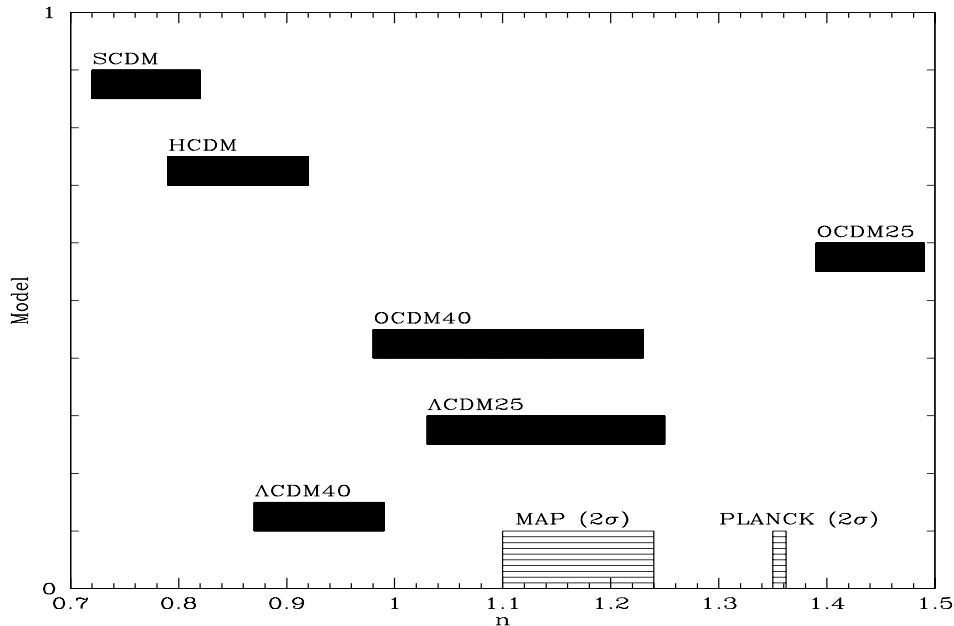


FIG. 15.— summarizes the model results on n when all the models are normalized to both COBE and local clusters, assuming that the primordial spectrum has a pure power law shape for the scales of cosmological interest ($\sim 1 - 6000h^{-1}\text{Mpc}$). The ranges in n are 2σ . Also shown are the 2σ errorbars that MAP and PLANCK are thought to be able to achieve (Zaldarriaga, Spergel, & Seljak 1997). Note that the horizontal locations of MAP and PLANCK indicators are arbitrary.

is cosmologically important but is not tangled with other complicated processes such as recombination and reionization processes, namely, the primordial power index n . Another reason for favoring the choice of n is that n is distinctly different between models and perhaps offers one of cleanest tests of models. The underlying reason that different models have distinctly different n is a product of combined effort: combining CMB (COBE) with local cluster observations. It is clearly seen from Table 1 that normalizing a model both to very large scale (COBE) and cluster scale results in a tight constraint on the primordial power spectrum index n . However, currently COBE does not provide strong constraint on n due to its large errorbars [$\Delta n = 0.6$ (2σ)]. In the foreseeable future there are two satellite missions, MAP and PLANCK, which are proposed to produce much higher resolution (arminute to sub-degree versus $\sim 10^\circ$ of COBE) and much more sensitive CMB temperature fluctuation measurements.

We summarize the model results on n in Figure 15. The ranges in n are 2σ . Also shown are the 2σ errorbars that MAP and PLANCK are thought to be able to achieve (Zaldarriaga, Spergel, & Seljak 1997). Note that the horizontal locations of MAP and PLANCK indicators are arbitrary. It is seen that MAP will be able to provide a powerful discriminator between the models, whereas PLANCK should be able to constrain n thus test models with exquisite precision.

4. DISCUSSION

When models are normalized to both COBE on very large scales and clusters of galaxies on intermediate-to-large scales, They naturally have grossly similar properties of clusters of galaxies at zero redshift. Other local tests

surrounding clusters regions or weighted heavily by clusters are unlikely to be very sensitive for the purpose of differentiating between models. Among such tests are galaxy-galaxy pairwise velocity dispersion (e.g., Davis & Peebles 1983; Strauss, Ostriker, & Cen 1998), galaxy-galaxy two point correlation function (Davis & Geller 1976; Peebles 1980) and large-scale velocity flows in the local universe (e.g., Strauss et al. 1995). Although it is conceivable that fine details within the clusters at zero redshift may differ among different models, such as cluster morphology, substructure etc. (Richstone, Loeb, & Turner 1992; Mohr et al. 1995; see Cen 1997b for a somewhat more realistic view on this considering some unavoidable projection effects), it is likely that more significant differences between the models will come from regions far removed from local clusters of galaxies. There are two ways to be distant from clusters. First, one can move to regions such filaments or voids in the local universe which are spatially distant from the clusters. There is no doubt that there are significant differences in the properties of these regions among different models. But detailed modeling of such regions, in particular, voids, is extremely difficult due to the lack of appropriate small scale resolution in such regions even with the best simulations available. We have followed on the second route in this paper by traveling back in time away from the local universe and studied the properties of model universes at moderate-to-high redshift through a suite of cosmological phenomena.

In addition to a consideration of galaxy power spectrum from SDSS galaxy redshift survey (§3.2), which is shown to be capable of differentiating between models, we have examined eight phenomena ranging in redshift from zero to that of last scattering. They include the correlation func-

tion of very rich clusters of galaxies (§3.1), the evolution of the abundance of rich clusters of galaxies (§3.3), the gravitational lensing by moderate redshift clusters of galaxies (§3.4), the properties of Ly α forest at high redshift (§3.5), the damped Ly α systems at high redshift (§3.6), the high redshift galaxies (§3.7), the reionization epoch of the universe (§3.8) and the future high resolution, high sensitivity CMB experiments (§3.9). Some of these observations have already provided discriminating tests between some models. For example, HCDM model is strongly ruled out by the observed large density of neutral hydrogens in damped Ly α systems and possibly inconsistent with observations of Ly α clouds. Both $\Omega_0 = 1$ tCDM and HCDM models are in disagreement with the observed abundance of rich clusters of galaxies at $z \sim 0.4 - 0.8$ and the observed strong clustering of high redshift galaxies at $z \sim 3$, while other, low density models are in fair agreement with those observations.

We find that all these moderate-to-high redshift phenomena possess potentially very powerful capabilities of differentiating between all the remaining “viable” models. We now discuss the requisite condition for each phenomenon to be capable of providing some useful constraint.

It is found that different models differ most for correlations of very rich clusters of galaxies, those with mean separation $\geq 90h^{-1}\text{Mpc}$. Let us take the data point shown as a solid dot in Figure 3 as an example to quantify this. If the errorbar were $2h^{-1}\text{Mpc}$ (1σ) (with the mean value unchanged), all the models may be ruled out at 4σ confidence level. Is this achievable? The answer is a probable yes with SDSS. Let us assume that the correlation function is a powerlaw with a slope of -1.8 . Then, the mean correlation function has a value $\xi(r_0) = 3\xi(r_0)/(3 - 1.8) = 2.5$ at r_0 (where the correlation function has a value unity). In order to achieve a statistical errorbar of $2h^{-1}\text{Mpc}$ for $r_0 = 42h^{-1}\text{Mpc}$, $N_{pair} = (42/2)^2 = 442$ pairs of clusters are necessary. Since $\bar{\xi} = N_{pair}/(V_{survey}n) - 1 = 2.5$ at r_0 , we get $V_{survey} = N_{pair}/3.5n = 1.0 \times 10^8 h^{-3}\text{Mpc}^3$ [$n = (1/94)^3 h^3\text{Mpc}^{-3}$ is assumed]. The SDSS survey volume is about $\frac{4\pi}{3}500^3 = 5.2 \times 10^8 h^{-3}\text{Mpc}^3$. So it seems that clusters from SDSS will provide an unprecedented accuracy for the determination of cluster correlations of very rich clusters.

The evolution rates of the abundances of rich clusters of galaxies in different models are quite different and differences of the abundances of clusters increasingly deviate from one another towards high redshift (Figure 7). As shown earlier, even the currently available very small data set is already able to differentiate the Ω_0 models (tCDM, HCDM) from the rest. However, larger cluster samples will be required to constrain Ω_0 to a high accuracy. As shown §3.3, a high redshift X-ray cluster survey covering a quarter of the sky with enough sensitivity to measure the temperature of hot luminous clusters ($kT \geq 7\text{keV}$) at $z \geq 1$ will be able to determine Ω_0 with an uncertainty of $\Delta\Omega_0 = 0.02$ (1σ), if $\Omega_0 + \Lambda_0 = 1$, and $\Delta\Omega_0 = 0.008$, if $\Lambda_0 = 0$. These accuracies are comparable to those which will be determined from the next generation microwave background fluctuation experiments (e.g., Zaldarriaga, Spergel, & Seljak 1997), thus provides a very powerful cosmological test and also a very important con-

sistency cross-check.

The gravitational lensing optical depths for large splittings or giant arcs due to moderate-to-high redshift clusters of galaxies increasingly differ towards high redshift between models. While this is closely related to the evolution of abundance of rich clusters, the differences between different models tend to be larger and more extreme because of the highly nonlinear dependence of gravitational lensing cross section on cluster mass. For background sources at $z \leq 1$, the primary differences occur between models with different Ω_0 ; models with a same Ω_0 but with and without a cosmological constant give comparable results (Figure 9a). For background sources at $z \sim 3$, all the models become non-degenerate (Figure 9b). A systematic search of about 10^6 background sources at $z \geq 3$ will be desirable. In fact, SDSS should provide such a sample ($\sim 10^6$ quasars mostly at high redshift with photometric redshifts and 10^5 quasars with spectroscopic redshifts, Margon 1998). One can use such a sample in two ways. Firstly, the total number of lensed sources will be different between the models. With 10^6 quasars (assuming to be at $z_s = 3$ for this simple illustration), one should see (1900 ± 44 , 710 ± 27 , 570 ± 24 , 330 ± 18 , 100 ± 10 , 39 ± 6) multiple-image quasars with separation $\geq 30''$ in (OCDM25, OCDM40, Λ CDM25, Λ CDM40, tCDM, HCDM), respectively. This would allow an unambiguous test of these six models. It would put a constraint on Ω_0 with $\Delta\Omega_0 \sim 0.01$ if the universe is open or $\Delta\Omega_0 \sim 0.03$ if the universe is flat. Secondly, and more sensitively, the distributions of lenses themselves in different models will be very different. For example, one expect to see (200.0, 4.0, 0.5, 0.005, 0.0, 0.0) lenses at $z > 2$ in (OCDM25, OCDM40, Λ CDM25, Λ CDM40, tCDM, HCDM), respectively, that produce arcs or splittings $\geq 30''$.

The properties of Ly α forest at high redshift are likely to be dramatically different among the models given the order of magnitude different powers on the relevant scales. With regard to this, observations are perhaps slightly ahead of theory; there is a large and still rapidly accumulating observational database for Ly α forest. But detailed hydrodynamic simulations of Ly α forest, while having made ground-breaking advances in our understanding of Ly α forest phenomenon in recent years, are yet to sort out the fine dependence of results on such issues as variations among different hydrocodes, resolution and boxsize effect, radiative transfer effect and star formation feedback effects, before they can be utilized to test cosmological models in accurate (thus meaningful) ways. Preliminary comparisons between models and observations using the one-point flux distribution probability function (Rauch et al. 1997) favor the two Λ based models (Λ CDM25 and Λ CDM40), but disfavor HCDM and OCDM25 in the opposite sense that HCDM has too little power and OCDM25 has too much power on the relevant scales. tCDM and OCDM40 appear to be marginally consistent.

The neutral hydrogen mass in damped Ly α systems at high redshift is undoubtedly a very sensitive test. Their role is comparable to that of rich clusters today in the sense that damped Ly α systems are rare systems at the high redshift. Four improvements will dramatically enhance its discriminatory power. First, more detailed kinematic studies of these systems, at the highest redshift possible, are indispensable to providing more tight limits on

the mass of these systems. Second, a significant reduction of observational errorbars with more samples can significantly increase the sensitivity of the test. SDSS should provide a much larger quasar sample. Third, it is beneficial to go to higher redshift to further increase its sensitivity of testing cosmological models. Finally, detailed modeling of these systems is necessary in order to determine the precise amount of gas in neutral form. For this we will have to implement detailed three-dimensional radiative transfer in the existing hydrocodes, run large simulation boxes ($\geq 20h^{-1}\text{Mpc}$) to ensure a fair sample and have a better understanding of the star formation processes in these systems.

The abundance and clustering of high redshift galaxies at $z \sim 3$ has been shown to differ among models. These are the large proto-clusters or proto-superclusters that eventually produce the clusters and superclusters of galaxies that we see today. The issue here is to enlarge the observational sample size. If the observed galaxy concentration seen by S98 turns out to be ubiquitous, all the models considered would be in a very uncomfortable position. With about ten fields like SSA22, preferably randomly distributed spatially, we may be able to reject some models with high confidence levels. A perhaps more discriminatory test with the high redshift galaxies is from measuring the velocity dispersion (or mass) of these galaxies. If the high redshift galaxies are as massive as the present day L^* galaxies, as present preliminary observational evidence indicates (Steidel et al. 1996), all $\Omega_0 = 1$ models are inviable.

The reionization epoch of the universal baryons is shown to be substantially different among the models. It is very worthwhile to search for quasars at as high redshift as possible. For example, if quasars can be seen beyond $z > 5$, HCDM will be inviable; if quasars can be seen beyond $z > 10$, only low density open models could pass. Next generation infrared telescopes such as SIRTF and NGST and next generation radio telescopes such as GMRT and SKAI will prove to be extremely useful to not only test the models but also understand the detailed history of the reionization. Future CMB experiments will also shed light on this.

Finally, the future high resolution, high sensitivity CMB experiments such as MAP and PLANCK will provide many sensitive tests. Among them one critical test will be an unambiguous determination of the primordial power index. Accurate determinations by MAP and PLANCK will provide strong constraints on Ω_0 .

5. CONCLUSIONS

We examine a set of observations and compare them (if currently available) with a set of six COBE and cluster normalized CDM models, or forecast their capabilities in constraining models or outline the requirements for them to be capable of constraining models in a dramatic fashion. Detailed discussion has been presented in the previous section. In addition to SDSS galaxy redshift survey (§3.2), we have examined eight different phenomena including the correlation function of very rich clusters of galaxies (§3.1), the evolution of abundance of rich clusters of galaxies (§3.3), the gravitational lensing by moderate-to-high redshift clusters of galaxies (§3.4), the properties of Ly α forest (§3.4), the damped Ly α systems at high red-

shift (§3.6), the high redshift galaxies (§3.7), the reionization epoch of the universal baryons (§3.8) and the future high resolution, high sensitivity CMB experiments (§3.9). Some of these observations have already provided discriminating tests on some models.

The hot+cold dark matter model (with $\Omega_h = 0.2$) is already ruled out at a $> 3\sigma$ level by current observations of damped Ly α systems at high redshift and the observed high abundance of rich clusters of galaxies at $z \sim 0.4 - 0.8$. There is some preliminary indication that there is not enough power in HCDM to account for the observed high redshift galaxies and the Ly α forest lines. HCDM is marginally consistent with the existence of $z \sim 5$ quasars in the sense that the HCDM universe would be marginally completely reionized by $z \sim 5$; seeing higher redshift quasars will be an embarrassment to HCDM. Overall, HCDM is the least viable model among examined and is ruled out in several independent ways at high confidence levels.

The tilted CDM model (tCDM) is in disagreement with the observed high abundance of rich clusters of galaxies at $z \sim 0.4 - 0.8$ at a high confidence level ($> 3\sigma$). It is inconsistent with the observed strong correlation of clusters of galaxies — another manifestation of lack of large-scale power of the model (even with a substantial tilt, as is required to fit both COBE and local cluster abundance and included in the analysis). tCDM is marginally inconsistent ($\sim 1 - 2\sigma$) with the observations of damped Ly α systems in the sense that it underpredicts the amount of neutral hydrogen in damped Ly α systems at $z \sim 3 - 4$, but is marginally consistent with the observed flux distribution of Ly α forest. In summary, tCDM does not seem to be favored.

Low density, flat CDM models with a cosmological constant are consistent with all the observations examined here with the preferred range of the density parameter being $\Omega_0 = 0.30 \pm 0.10$. This preferred range is primarily constrained at the high end by the abundance of clusters of galaxies at $z \sim 0.5$ (in order not to underproduce the cluster abundance) and at the lower end by the flux distribution of Ly α forest at $z \sim 2$ (in order not to overproduce the fluctuations in the flux distribution) and also by observations of the damped Ly α systems $z \sim 3$ (in order not to overproduce the abundance of damped Ly α systems).

Low density, open CDM models are consistent with all the observations examined that are currently available with the preferred density range being $\Omega_0 = 0.45 \pm 0.10$, which is constrained by similar observations aforementioned in the preceding paragraph for the Λ CDM models. An additional constraint is provided by the observed galaxy fluctuations in the local universe, $\sigma_8(gal) \sim 1.0$. Since it is improbable for galaxies to be anti-biased tracers of the mass, $\sigma_8(gal) \sim 1.0$ (Strauss & Willick 1995) implies $\sigma_8(mass) \leq 1.0$, which translates into an requirement $\Omega_0 \geq 0.25$ for open CDM models.

Some improvements on the comparisons between models and observations will be likely in a relatively short term, either through more realistic modeling and/or by improved observational data, including the correlation function of very rich clusters of galaxies at $z=0$ (from SDSS), the Ly α forest at $z \sim 2 - 4$ (primarily by more careful modeling and analysis), damped Ly α systems (by Keck) and high redshift galaxies at $z \sim 3$ (using Keck and others).

These observations look at different physical scales of a model at different redshift: the correlation function of very rich clusters of galaxies probes the power on large scales, $\lambda \geq 100h^{-1}\text{Mpc}$, at $z = 0$; the Ly α forest lines measure the power on small scales, $\lambda \sim 0.1h^{-1}\text{Mpc}$, at $z \sim 2 - 4$; the damped Ly α systems check the power on intermediate scales, $\lambda \sim 1.0h^{-1}\text{Mpc}$, at $z \sim 3$; and the abundance and clusters of the high redshift galaxies constrain the power on intermediate-to-large scales, $\lambda \sim 1.0 - 100h^{-1}\text{Mpc}$, at $z \sim 3$. These improvements will further tighten the parameter space for the low density models.

The evolution rates of the abundances of rich clusters of galaxies in different models are quite different and differences of the abundances of clusters increasingly deviate from one another towards high redshift. A large and deep X-ray cluster survey would be invaluable to determine the abundance of high redshift, hot and luminous X-ray clusters, which would permit an accurate determination of Ω_0 . A large survey covering about a quarter of the sky and capable of detecting hot and luminous clusters ($kT \geq 7\text{keV}$) at $z \geq 1.0$ would place a constraint on Ω_0 with $\Delta\Omega_0 \sim 0.01$. These accuracies are comparable to those which will be determined from the next generation microwave background fluctuation experiments (e.g., Zaldarriaga, Spergel, & Seljak 1997), thus provide a very powerful test and also a very important consistency cross-check. While AXAF will provide a deep sample of X-ray clusters of galaxies, a larger survey is required to make a competitively accurate constraint on Ω_0 .

Gravitational lensing observations of giant arcs or very large splitting multiple quasars by clusters of galaxies will provide very sensitive tests. For the same reason that cluster abundances at high redshift are different in different models, gravitational lensing provides an independent measurement of the same objects – rich clusters of

galaxies at moderate to high redshift – as well as lensed high redshift sources. The quasar data set from SDSS may permit an unprecedented, accurate determination of both the lensing optical depth and the redshift distribution of the lenses themselves (perhaps in conjunction with follow-up observations to determine the redshifts of high redshift lenses). A very tight constraint can be placed on Ω_0 with $\Delta\Omega_0 \sim 0.01$.

Observation of the reionization of the universe would provide the potential to differentiate between open and Λ CDM models. Perhaps the simplest discriminator will be to sight a very high redshift quasar $z > 10$. If such a quasar is seen, open models will be preferred.

A combination of several (or all) of the aforementioned observations will offer several ways to break the current degeneracy of models that are both COBE and cluster normalized, primarily between open CDM and Λ CDM models. On the other hand, any conflict among the observations with respect to all the models may have profound implications with respect to the Gaussian picture of structure formation and/or the general gravitational instability theory.

The work is supported in part by grants NAG5-2759 and ASC93-18185. Discussions with Drs. N. Bahcall, J.R. Bond, M. Dickinson, G. Lake, J.P. Ostriker, D.N. Spergel and M.A. Strauss are gratefully acknowledged. D. Goldberg and M. Strauss are thanked for supplying the SDSS power spectrum results. Special thanks are extended to an anonymous referee who made several helpful comments. Finally, I would like to thank George Lake and University of Washington for the warm hospitality, and financial support from the NASA HPCC/ESS Program during a visit when this work was initiated.

REFERENCES

- Adams, F., Bond, J.R., Freese, K., Frieman, J. & Olinto, A., 1993, preprint
- Albrecht, A. & Steinhardt, P.J. 1982, Phys. Rev. Lett., 48, 1220
- Bahcall, N.A., & Cen, R. 1992, ApJ, 398, L81
- Bahcall, N.A., & Cen, R. 1993, ApJ, 407, L49 (BC)
- Bahcall, N.A., Fan, X., & Cen, R. 1997, ApJ, 485, L53
- Bahcall, N.A., & Soneira, R.M. 1983, ApJ, 270, 20
- Bahcall, J.N., et al. 1996, ApJ, 457, 19
- Bagla, J.S. 1998, MNRAS, 297, 251
- Bartelmann, M., Huss, A., Colberg, J.M., Jenkins, A., & Pearce, F.R. 1997, preprint, astro-ph/9707167
- Blanton, M., Cen, R., Ostriker, J.P., & Strauss, M.A. 1998, preprint
- Blumenthal, G.R., Faber, S.M., Primack, J.R., & Rees, M.J. 1984, Nature, 311, 517
- Braun, R. 1995, in The Westerbork Observatory, Continuing Adventure om Radio Astronomy, p167
- Bryan, G.L., Cen, R., Norman, M.L., Ostriker, J.P., & Stone, J.M. 1994, ApJ, 428, 405
- Bucher, Goldhaber, & Turok, N. 1995, preprint
- Burles, S., & WTytler, D. 1997, preprint, astro-ph/9712108
- Carlberg, R.G., Morris, S.M., Yee, H.K.C., & Ellingson, E. 1997, ApJ, 479, L19 (C97)
- Cen, R. 1992, ApJS, 78, 341
- Cen, R. 1994, ApJ, 437, 12
- Cen, R. 1997a, ApJ, 479, L85
- Cen, R. 1997b, ApJ, 485, 39
- Cen, R. 1997c, ApJ, 491, 1
- Cen, R. 1998, ApJ, in press (C98)
- Cen, R., Bahcall, N.A., & Gramann, M. 1994, ApJ, 437, L51
- Cen, R., Gnedin, N.Y., Kofman, L.A., & Ostriker, J.P. 1992, ApJ, 399, L11
- Cen, R., Gnedin, N.Y., & Ostriker, J.P. 1993, ApJ, 417, 387
- Cen, R., & Ostriker, J.P. 1992a, ApJ, 393, 22
- Cen, R., & Ostriker, J.P. 1992b, ApJ, 399, L113
- Cen, R., & Ostriker, J.P. 1993, ApJ, 417, 404
- Cen, R., & Ostriker, J.P. 1993, ApJ, 417, 415
- Cen, R., & Ostriker, J.P. 1994a, ApJ, 429, 4
- Cen, R., & Ostriker, J.P. 1994b, ApJ, 431, 451
- Cen, R., Gott, J.R., III, Ostriker, J.P., & Turner, E.L. 1994, ApJ, 423, 1
- Cen, R., Ostriker, J.P., & Peebles, P.J.E. 1993, ApJ, 415, 423
- Cen, R., & Ostriker, J.P. 1998, in preparation
- Cen, R., Phelps, S., Miralda-Escudé, J., & Ostriker, J.P. 1998, ApJ, 496, 577
- Crittenden, R., Bond, J.R., Davis, R.L., Efstathiou, G., & Steinhardt, P.J. 1993, Phys. Rev. Lett., 71, 324
- Croft, R.A.C., & Efstathiou, G. 1994, MNRAS, 267, 390
- Dalton, G.B., Efstathiou, G., Maddox, S.J., & Sutherland, W.J. 1992, ApJ, 390, L1
- Dalton, G.B., Croft, R.A.C., Efstathiou, G., Sutherland, W.J., Maddox, S.J., & Davis, M. 1994, MNRAS, 271, L47
- Danos, R., & Pen, U. 1998, preprint, astro-ph/9803058
- Davis, M., & Geller, M.J. 1976, ApJ, 208, 13
- Davis, M. Efstathiou, G., Frenk, C.S., & White, S.D.M. 1985, ApJ, 292, 371
- Davis, M., & Peebles, P.J.E. 1983, ApJ, 267, 465
- Davis, M., Summers, F.J., & Schlegel, D. 1992, Nature, 359, 393
- Davis, R.L., Hodges, H.M., Smoot, G.F., Steinhardt, P.J., Turner, M.S. 1992, Phys. Rev. Lett., 69, 1856; erratum, 70, 1733
- Edge, A.C., et al. 1994, A&A, 289, L34
- Efstathiou, G., Bond, J.R., & White, S.D.M. 1992, MNRAS, 258, 1p
- Efstathiou, G. P. 1992, MNRAS, 256, 43p
- Efstathiou, G., & Bond, J.R., preprint, astro-ph/9807103
- Fan, X., Bahcall, N.A., & Cen, R. 1998, ApJ, 490, L123
- Frenk, C.S., White, S.D.M., Davis, M., & Efstathiou, G. 1988, ApJ, 327, 507
- Fukugita, M., & Turner, E.L. 1991, MNRAS, 253, 99
- Gnedin, N.Y., & Ostriker, J.P. 1997, 486, 581

- Goldberg, D.M., & Strauss, M.A. 1998, ApJ, 495, 29
- Gott, J.R., III 1982, Nature, 295, 304
- Governato, F., Baugh, C.M., Frenk, C.S., Cole, S., Lacey, C.G., Quinn, T., & Stadel, J. 1998, preprint, astro-ph/9803030
- Gramann, M., Cen, R., & Bahcall, N.A. 1993, ApJ, 419, 440
- Gramann, M. & Einasto, J. 1992, MNRAS, 254, 453
- Haiman, Z., & Loeb, A. 1997, ApJ, 483, 21
- Henry, J.P., & Arnaud, K.A. 1991, ApJ, 372, 410
- Hernquist, L., Katz, N., & Weinberg, D.H. 1996, ApJ, 457, L51
- Hu, E. M., Kim, T.-S., Cowie, L. L., Songaila, A., & Rauch, M. 1995, AJ, 110, 1526
- Jing, Y.P., & Suto, Y. 1998, ApJ, 494, L5
- Kaiser, N. 1987, MNRAS, 227, 1
- Kaiser, N., & Squires, G. 1993, ApJ, 404, 441
- Kang, H., Cen, R., Ostriker, J.P., & Ryu, D. 1994, ApJ428, 1
- Kauffman, G., & Charlot, S. 1994, ApJ, 430, L97
- Klypin, A., Holtzman, J., Primack, J., & Regos, E. 1993, ApJ, 416, 1
- Klypin, A., Borgani, S., Holtzman, J., & Primack, J. 1995, ApJ, 444, 1
- Kofman, L.A., Gnedin, N.Y., & Bahcall, N.A. 1993, ApJ, 413, 1
- Lanzetta, K.M., Bowen, D.V., Tytler, D., & Webb, J.K. 1995a, ApJ, 442, 538
- Lanzetta, K.M., Wolfe, A.M., & Turnshek, D.A. 1995b, ApJ, 440, 435 (L95)
- Le Fevre, O., Hammer, F., Angonin, M.C., Gioia, I.M., & Luppino, G.A. 1994, ApJ, 422, L5
- Liddle, A.R., & Lyth, D.H. 1992, Phys. Lett., B 291, 391
- Liddle, A.R., Lyth, D.H., & Sutherland, W. 1992, Phys. Lett., B 279, 244
- Lidsey, J.E., Coles, P. 1992, MNRAS, 258, 57p
- Linde, A. 1982, Phys. Lett, 108B, 389
- Lowenthal, J.D., Koo, D.C., Guzman, R., Gallego, J., Phillips, A.C., Faber, S.M., Vogt, N.P., Illingworth, G.D., & Gronwall, C. 1997, ApJ, 481, 673
- Lu, L., Sargent, W.L.W., & Barlow, T.A. 1997, ApJ, 484, 131
- Lubin, L.M., Cen, R., Bahcall, N.A., & Ostriker, J.P. 1996, ApJ, 460, 10
- Lucchin, F., Matarrese, S., & Mollerach, S. 1992, ApJ, 401, L49
- Lumsden, S.L., Nichol, R.C., Collins, C.A., & Guzzo, L. 1992, MNRAS, 258, 1
- Luppino, G.A., & Gioia, I.M. 1995, ApJ, 445, 77 (LG95)
- Ma, C.P., & Bertschinger, E. 1994, ApJ, 435, L9
- Ma, C.P., Bertschinger, E., Hernquist, L., Weinberg, D.H., & Katz, N. 1997, ApJ, 484, L1
- Madau, P., Meiksin, A., & Rees, M.J. 1997, ApJ, 475, 429
- Maddox, S.J., Efstathiou, G., Sutherland, W.J., & Loveday, J. 1990, MNRAS, 242, 43p
- Mao, S. 1991, ApJ, 380, 9
- Maoz, D., Rix, H.-W., Gal-Yam, A., Gould, A. 1997, ApJ, 486, 75
- Margon, B. 1998, preprint, astro-ph/9805314
- Miralda-Escudé, J. 1991, ApJ, 370, 1
- Miralda-Escudé, J., Cen, R., Ostriker, J. P., & Rauch, M. 1996, ApJ, 471, 582
- Miralda-Escudé, J., & Rees, M. 1997, ApJ, 478, L57
- iralda-Escudé, J., Rauch, M., Sargent, W. L. W., Barlow, T. A., Weinberg, D. H., Hernquist, L., Katz, N., Cen, R., & Ostriker, J. P. 1997, Proceedings of the 13th IAP Astrophysics Colloquium, *Structure and Evolution of the Intergalactic Medium from QSO Absorption Line Systems* eds. P. Petitjean, S. Charlot (Editions Frontières: Paris), p. 155.
- Mo, H.J., & Miralda-Escudé, J. 1994, ApJ, 430, L25
- Mohr, J., Evrard, A.E., Fabricant, D.G., & Geller, M.J. 1995, ApJ, 447, 8
- Moore, B., Katz, N., Lake, G., Dressler, A., & Oemler, A., Jr. 1996, Nature, 379, 613
- Narayan, R., & White, S.D.M. 1988, MNRAS, 231, 97
- Navarro, J.F., Frenk, C.S., & White, S.D.M. 1996, ApJ, 462, 563
- Ostriker, J.P. 1993, ARAA, 31, 689
- Ostriker, J.P., & Cen, R. 1996, ApJ, 464, 27
- Ostriker, J.P., & Gnedin, N.Y. 1996, ApJ, 472, L63
- Ostriker, J.P., & Steinhardt, P. 1995, Nature, 375, 274
- Park, C.B. 1990, MNRAS, 242, 59
- Peacock, J., & West, M. 1992, MNRAS, 259, 494
- Peebles, P.J.E. 1980, *The Large-Scale Structure of the Universe* (Princeton: Princeton University Press)
- Peebles, P.J.E. 1982, ApJ, 263, L1
- Peebles, P.J.E. 1984, ApJ, 284, 439
- Peebles, P.J.E. 1987a, Nature, 327, 210
- Peebles, P.J.E. 1987b, ApJ, 315, L73
- Peebles, P.J.E. 1993, *The Principles of Physical Cosmology* (Princeton: Princeton University Press)
- Peebles, P.J.E., Daly, R.A., & Juskiewicz, R. 1989, ApJ, 347, 563
- Pen, U.-L. 1996, preprint, astro-ph/9610147
- Pettini, M., Steidel, C.C., Adelberger, K.L., Kellogg, M., Dickinson, M., & Giavalisco, M. 1997, preprint, astro-ph/9708117
- Postman, M., Huchra, J.P., & Geller, M.J. 1992, ApJ, 384, 404
- Press, W. H., Rybicki, G. B., & Schneider, D. P. 1993, 414, 64
- Press, W.H., & Schechter, P.L. 1974, ApJ, 215, 703
- Prochaska, J.X., & Wolfe, A.M. 1997, ApJ, 487, p73
- Quinn, T., Katz, N., & Efstathiou, G. 1996, MNRAS, 278, L49
- Rauch, M., Carswell, R. F., Chaffee, F. H., Foltz, C. B., Webb, J. K., Weymann, R. J., Bechtold, J., & Green, R. F. 1992, ApJ, 390, 387
- Rauch, M., Miralda-Escudé, J., Sargent, W. L. W., Barlow, T. A., Weinberg, D. H., Hernquist, L., Katz, N., Cen, R., Ostriker, J. P., 1997, ApJ, 489, 7
- Reichart, D.E., Nichol, R.C., Castander, F.J., Burke, D.J., Romer, A.K., Holden, B.P., Collins, C.A., & Ulmer, M.P. 1998, preprint, astro-ph/9802153
- Richstone, D., Loeb, A., & Turner, E.L. 1992, ApJ, 393, 477
- Rosti, P., Dellaceca, R., Norman, C., & Giacomoni, R. 1998, ApJ, 492, 21
- Ryu, D., Ostriker, J. P., Kang, H., & Cen, R. 1993, ApJ, 414, 1
- Salaris, M., Degl'Innocenti, S., & Weiss, A. 1997, ApJ, 479, 665
- Scalo, J.M. 1986, Fund. Cosmic Phys., 11, 1
- Schneider, D. P., et al. 1993, ApJS, 87, 45
- Scott, D., & Rees, M. 1990, MNRAS, 240, 510
- Smail, I., et al. , 1996, MNRAS, 277, 1
- Smoot, G.F. et al. 1992, ApJ, 396, L1.
- Steidel, C.C., Giavalisco, M., Pettini, M., Dickinson, M., & Adelberger, K.L. 1996, ApJ, 462, L17
- Steidel, C.C., Adelberger, K.L., Dickinson, M., Giavalisco, M., Pettini, M., & Kellogg, M. 1998, ApJ, 492, 428 (S98)
- Stewart, E., & Lyth, D.H. 1993, Phys. Lett. B, 302, 171
- Storrie-Lombardi, L.J., McMahon, R.G., & Irwin, M.J. 1996, MNRAS, 293, L79 (S96)
- Strauss, M.A., & Willick, J.A. 1995, Phys. Repor, 261, 271
- Strauss, M.A., Cen, R., Ostriker, J.P., Lauer, T.R., & Postman, M. 1995, ApJ, 444, 507
- Strauss, M.A., Ostriker, J.P., & Cen, R. 1998, ApJ, 494, 20
- Subramanian, K., & Padmanabhan, T. 1993, MNRAS, 265, 101
- Subramanian, K., & Padmanabhan, T. 1994, preprint, astro-ph/9402006
- Suto, Y., Cen, R., & Ostriker, J.P. 1992, 395, 1
- Swarup, G. 1984, Giant Meter-Wavelength Radio Telescope - Proposal, Radio Astronomy Center, TIFR, India
- Taylor, A.N., & Rowan-Robinson, M. 1992, Nature, 359, 396
- Trimble, V. 1997, "The Extragalactic Distance Scale" ed. M. Livio, M. Donahue & N. Panagia, p407
- Turner, E.L., Ostriker, J.P., & Gott, J.R. III 1984, ApJ, 284, 1 (TOG)
- Tyson, J.A. 1983, ApJ, 272, L135
- Tyson, J.A., Valdes, F., & Wenk, R.A. 1990, ApJ, 349, L1
- Tytler, D., Fan, X.-M., Burles, S., Cottrell, L., Davis, C., Kirkman, D., & Zuo, L. 1995, in *QSO Absorption Lines*, Proc. ESO Workshop, ed. G. Meylan (Heidelberg: Springer), p. 289
- Viana, P.T.P., & Liddle, A.R. 1996, MNRAS, 281, 323
- Vogele, M.S., Park, C., Geller, M.J., Huchra, J.P., & Gott, J.R., III 1994, ApJ, 420, 525
- Walker, T.P. et al. 1991, ApJ, 376, 51
- Werner, M.W., & Eisenhardt P. 1988, Astro. Lett. Comm., 27, 89
- West, M.J., Oemler, A., Jr., & Dekel, A. 1988, ApJ, 327, 1
- White, S.D.M., Frenk, C.S., Davis, M., & Efstathiou, G. 1987, ApJ, 313, 505
- White, S.D.M., Efstathiou, G., & Frenk, C.S. 1993a, MNRAS, 262, 1023 (WEF)
- White, S.D.M., Navarro, J.F., Evrard, A.E., & Frenk, C.S. 1993b, Nature, 366, 6454
- Wolfe, A. M. 1995, in ESO Workshop on QSO Absorption Lines, ed. G. Meylan (Berlin: Springer), 13
- Wambsgans, J., Cen, R., Ostriker, J.P., & Turner, E.L. 1995, Science, 268, 274
- Zaldarriaga, M., Spergel, D.N., & Seljak, U. 1997, ApJ, 488, 1
- Zel'dovich, Ya. B. 1980, MNRAS, 192, 663
- Zhang, Y., Anninos, P., & Norman, M.L. 1995, ApJ, 453, L57
- Zuo, L., & Lu, L. 1993, ApJ, 418, 601